Diplomarbeit

Two Independent Standardised Approaches to Quantify Chronic Sun Exposure in Human Skin Samples of Malignant Melanoma: Histological Staining of Solar Elastosis and Analysis of Loss of Autofluorescence in Elastic Fibres

eingereicht von

Gregor Mayer

zur Erlangung des akademischen Grades

Doktor der gesamten Heilkunde

(Dr. med. univ.)

an der

Medizinischen Universität Graz

ausgeführt am

QIMR Berghofer Medical Research Insitute, Brisbane

und an der

Universitätsklinik für Dermatologie und Venerologie, Graz

unter der Anleitung von

Prof. Peter Wolf

Prof. Werner Aberer

Dr. Elke Hacker (externe Betreuerin)

Prof. Nick Hayward (externer Betreuer)

Graz, 01.09.2015

Eidesstattliche Erklärung

Ich erkläre ehrenwörtlich, dass ich die vorliegende Arbeit selbstständig und ohne fremde Hilfe verfasst habe, andere als die angegebenen Quellen nicht verwendet habe und die den benutzten Quellen wörtlich oder inhaltlich entnommenen Stellen als solche kenntlich gemacht habe.

Graz, am 01.09.2015 *Gregor Mayer eh*

Preface

This thesis is the product of a seven-week research stay at the QIMR Berghofer Medical Research Insitute in Brisbane, Australia. The idea of investigating if the fluorescence pattern of H&E stained dermal elastic fibres correlates with the degree of accumulated solar exposure was established by Dr Elke Hacker. She generously offered to me to conduct the scientific laboratory work concerning this question.

During seven weeks at the QIMR I amended Dr Hacker's method and introduced another approach to quantify accumulated chronic sun damage in human skin by measuring the amount of solar elastosis in histological skin samples using a colour-based computer program.

I conducted the work under the immediate supervision of Laboratory Assistant Thomas Pollak and used the facilities of Prof Nick Hayward's Oncogenomics Laboratory.

Acknowledgements

Medical University of Graz

I would like to thank my supervisors Prof Peter Wolf (Department of Dermatology and Venereology) who helped me finalise this thesis and Prof Werner Aberer (Department of Dermatology and Venereology) for their support. Furthermore, I would like to thank Prof Jürgen Becker, my first supervisor of the Department of Dermatology and Venereology who initially agreed to participate in the cooperation between the Medical University of Graz and the QIMR Berghofer Medical Research Institute in Brisbane, Australia.

For statistical advice I would like to thank Prof Josef Haas (Department of Obstetrics and Gynaecology).

QIMR Berghofer Medical Research Institute

Special thanks to Dr Elke Hacker in Brisbane who allowed me to conduct a project based on her idea of creating an algorithm for the standardised quantification of the degree of chronic sun damage in human skin. I would also like to express my gratefulness for Prof Nick Hayward, head of the Oncogenomics Laboratory, and his entire laboratory staff for welcoming me in their facilities.

I am especially grateful for the support of Thomas Pollak, former Laboratory Assistant at the QIMR, who was my immediate supervisor and the first person to contact if any question occurred. Furthermore, he was fundamentally involved in the organisation of my research stay and he introduced me into the laboratory environment. Moreover, I want to thank Thomas and Elie for letting me stay with them and for a wonderful time in Brisbane during my time at the QIMR.

Furthermore, I would like to express special thanks to Prof David Whiteman who supplied me with tissue samples and patients' background information during and after my stay at the QIMR and hence enabled me to create a conclusive thesis.

For methodological advice I would like to thank Clay Winterford (Facility of Histotechnology) and Nigel Waterhouse (Flow Cytometry and Imaging Facility). I would like to emphasise the support of Glynn Rees (Facility of Histotechnology) whose advice had a major impact on my thesis. He helped me choose adequate staining methodologies, conducted staining procedures with hazardous substances, supplied me with excellent

methodological literature and gave me feedback on parts of my written thesis during and after my stay at the QIMR.

I am very grateful to have been given the opportunity to gain insight into professional scientific laboratory research and to have been able to express and pursue my own considerations with the generous support of the QIMR Berghofer Medical Research Institute and an overwhelming number of its gracious employees.

Finally, I would like to thank my friends, but especially my parents, Reinhold and Christiane Mayer, Karl Müller-Bruckschwaiger and the entire family Müller who have greatly supported and encouraged me in every aspect throughout my laboratory work, my writing, my entire medical studies and far beyond.

Table of content

Glossary and abbreviations

ACTH	Adrenocorticotropic hormone
AGE	Advanced glycation end product
AJCC	American Joint Committee on Cancer
AP-1	Activating protein 1
AUC	Area under the Curve
BCC	Basal cell carcinoma
BP	Band pass
CML	N^{ε}-(carboxymethyl)lysine
CSD	Chronic sun damage
DNA	Deoxyribonucleic acid
ECM	Extracellular matrix
FFPE	Formalin fixed, paraffin embedded
GAG	Glycosaminoglycan
GMS	Grocott's Method for Fungi
H&E	Hematoxylin and Eosin
HA	Hyaluronic acid
LMM	Lentigo maligna melanoma
LoFM	Loss of Fluorescence-Method
MM	Malignant melanoma
MMP	Matrix metalloproteinase
MS	Microsoft
mtDNA	Mitochondrial DNA
NA	Numerical aperture
NFκB	Nuclear factor kappa-light-chain-enhancer of activated B cells

NM	Nodular melanoma
OES	Orcein Elastin Stain
OES1; -2; -3:	Analysis algorithms of ImageScope's PPC feature applied on OES slides
PKCδ	Protein kinase C, isoform δ
PM	Positivity-Method
PPC	Positive Pixel Count; analysis feature of Leica's ImageScope
ROC	Receiver-operator characteristic
ROS	Reactive oxygen species
SCC	Squamous cell carcinoma
SSM	Superficial spreading melanoma
TGF-β	Transforming growth factor β
UV(R)	Ultraviolet (radiation)
UVA	Ultraviolet A (spectrum: 320-400nm wavelength)
UVB	Ultraviolet B (spectrum: 290-320nm wavelength)
α-MSH	α-melanocyte-stimulating hormone

List of illustrations

List of tables

Abstract

Sunlight as potentially hazardous radiation and a risk factor for the development of dermatological conditions such as non-melanoma skin cancer is well documented. The exact correlation between ultraviolet radiation and the pathogenesis of malignant melanoma, on the other hand, is still somewhat obscure, more complex and certainly does not follow a linear model.

The degree of the impact of accumulated solar irradiation onto skin is generally histologically assessed by experienced pathologists who usually subjectively assign the amount of solar elastosis in H&E stained skin samples to semiquantitative classes. A standardised quantitative approach to determine the degree of extrinsic skin aging in human specimens could be useful for epidemiological studies.

In this diploma thesis, two independent approaches to quantify the degree of extrinsic skin aging were established and tested in 49 samples of human cutaneous malignant melanoma from Australia: 1) A colour-based computer program quantified the amount of elastic fibres and elastotic bulk in specimens stained with Unna's Orcein Technique and Light Green (Positivity-Method, PM). 2) The loss of autofluorescent activity in superficial H&E stained elastic fibres at an excitation wavelength of 490nm was quantified (Loss of Fluorescence-Method, LoFM).

For both methods, threshold values were determined and tested for their accuracy in separating the specimens into three semiquantitative groups of chronic sun damage (CSD; "mild", "moderate" and "marked") which they were previously assigned to by microscopic examination at the hands of three collaborating Australian pathologists. Threshold values between classes mild and moderate CSD and between moderate and marked CSD were tested: For the PM and the LoFM, Youden's indexes of these threshold values were calculated at 0.727 (mild-moderate) and 0.869 (moderate-marked) and at 0.786 (mild-moderate) and 0.793 (moderate-marked), respectively. Furthermore, a Pearson product-moment correlation coefficient between the two methods was determined at 0.899.

The obtained statistical results indicate that both methods established in this thesis can be used to objectively quantify the degree of extrinsic skin aging in human skin. Hence, they represent reliable alternatives to the subjective and semiquantitative approach currently used in most of the medical research projects.

Zusammenfassung

Sonnenlicht als potentiell gesundheitsschädigende Strahlung und seine Rolle als Risikofaktor für die Entwicklung dermatologischer Erkrankungen wie Nichtmelanom-Hautkrebsarten sind ausführlich festgehalten. Der genaue Zusammenhang zwischen UV-Strahlung und der Entwicklung des Malignen Melanoms folgt allerdings keinem einfachen linearen Gesetz und konnte trotz intensiver wissenschaftlicher Anstrengungen immer noch nicht restlos geklärt werden.

Der Grad des Ausmaßes akkumulierter Sonnenexposition von Haut wird heutzutage üblicherweise an HE-gefärbten histologischen Schnitten von erfahrenen Pathologen beurteilt und in semiquantitative Kategorien eingeteilt. Eine standardisierte vollquantitative Methode zur Bestimmung des Ausmaßes chronischen Hautschadens könnte für eine Reihe von epidemiologischen Fragestellungen von Interesse sein.

In dieser Diplomarbeit wurde die Verlässlichkeit zweier neu erstellter, voneinander unabhängiger Quantifizierungsmethoden des Ausmaßes der akkumulierten Sonnenbestrahlung an 49 kutanen Melanom-Präparaten aus Australien untersucht: 1) Ein farbgesteuertes Computerprogramm quantifizierte die Menge elastischen und elastotischen Materials in Hautproben, die mittels Unna's Orcein Technique und Light Green gefärbt wurden (Positivity-Method, PM). 2) Der Grad des Verlusts an Autofluoreszenz HE-gefärbter, oberflächlicher elastischer Fasern unter einer Bestrahlungswellenlänge von etwa 490nm wurde quantifiziert (Loss of Fluorescence-Method, LoFM).

Für beide Methoden wurden Grenzwerte zur Trennung dreier semi-quantitativer Hautproben-Gruppen unterschiedlichen Ausmaßes akkumulierter Sonnenbestrahlung („mild", „moderat" und „stark") berechnet und auf Ihre Verlässlichkeit getestet. Im Vorfeld teilten nach mikroskopischer Begutachtung drei kollaborierende australische Pathologen die Proben den oben genannten Gruppen zu. Grenzwerte zwischen den Klassen „milden" und „moderaten" Ausmaßes und den Klassen „moderaten" und „starken" Ausmaßes an akkumulierter Sonnenbestrahlung wurden getestet: Für die PM wurden Youden Indexe von 0,727 (Grenzwert mild-moderat) und 0,869 (Grenzwert moderat-stark), für die LoFM von 0,786 (mild-moderat) und 0,793 (moderat-stark) berechnet. Darüber hinaus wurde ein Produkt-Moment-Korrelationskoeffizient von 0,899 zwischen den Methoden PM und LoFM ermittelt.

Die ermittelten statistischen Werte zeigen, dass beide in dieser Arbeit getesteten Methoden verlässliche Alternativen zur derzeit gewöhnlich angewandten subjektiven und semiquantitativen Quantifizierung chronischer Sonnenexposition durch erfahrene Pathologen darstellen. Darüber hinaus stellen die PM und die LoFM durch ihren vollquantitativen Charakter und ihre Objektivität standardisierte und dadurch vergleichbare Verfahren dar.

1 Introduction

This section describes physiological and pathophysiological entities and processes of the human skin and emphasises information which provides basal understanding of my investigations and interpretations. I will leave out large chapters of the skin but provide an overview of its anatomy and functional characteristics in order to make this thesis a conclusive and comprehensible work.

1.1 Physiological structure of the skin

As the cover of the human body the skin provides protection against thermal, mechanical and chemical hazards and ultraviolet radiation (UVR). It comprises a number of immunocompetent cells which keep the human body safe from infectious agents, allowing us to interact with our surrounding by using this organ's subtle tactile sense. (1,2) Furthermore, the skin participates in the process of vitamin D synthesis and thus also plays an important endocrine role. (3)

Roughly 2 square metres in total surface the skin is structured in three main layers: the epidermis, the dermis and the subcutaneous fatty tissue (also known as hypodermis). (1)

The **epidermis** constitutes the surface of the skin; it is an epithelial tissue and as such it mostly consists of cells situated tightly next to each other with very little extracellular space. Keratinocytes, which make up most of the epidermis, create a multilayered cornified squamous epithelium by proliferating at its base and keratinising in superficial layers. Besides keratinocytes the epidermis also hosts melanocytes which synthesise pigment (melanin) and distribute it to the keratinocytes so they can protect their nuclei from UVR, Langerhans' cells which represent remote agents of the immune system and Merkel cells which are part of the sensory system and mainly perceive pressure. (1,2)

The epidermis is structurally divided from the dermis by a fibrillary boundary, referred to as **basement membrane**. This membrane creates a two-dimensional web following a wavy course between epidermal rete ridges and dermal papillae (see below) and consists of two parts: the basal lamina facing the epidermis and the reticular lamina beneath. The basal lamina mainly contains collagen IV and laminin; collagen ensures mechanical stability while laminin helps creating a connection with the basal keratinocytes via anchoring proteins like integrin. The main structural component of the reticular lamina is collagen III,

among many other molecules. The connection between these two laminae is provided by collagen VII. Of course, this description depicts a simplified model of the complex construction of basement membranes. (2)

The **dermis** consists of fibroblasts and their product, the extracellular matrix (ECM). In contrast to the epidermis the ratio between ECM and cells is shifted towards the ECM. The biomechanical characteristics of the dermal extracellular fibrous network provide the skin with tensile strength and elasticity. Since the composition of the ECM is of special interest for this thesis I will go into further detail about it in *Section 1.1.1*. The dermis can be subdivided into two layers: the papillary dermis which is situated right beneath the epidermis and the deeper reticular dermis. The papillary dermis and the epidermis create extensions which interdigitate and hence contribute to the wavy course of the basement membrane: The papillary dermis creates dermal papillae which extend into the direction of the skin's surface and in-between of epidermal rete ridges. (1,2)

The papillary dermis is rich in small vessels and comprises more cells than the reticular dermis which has a dense network of fibres and greatly contributes to the mechanical resilience of the skin. Furthermore, the dermis contains two kinds of mechanoreceptors: Ruffini corpuscles which are attached to collagen fibres and sense distension and Meissner's corpuscles which can be found in the dermal papillae of the hairless skin and play a crucial role for the sensitive perception of touch at finger pads. (1,2)

The **hypodermis** consists of loose connective tissue which comprises a lot of adipocytes. This skin layer decreases the transmission of mechanical forces from the skin into the depth. It creates a connection between the skin and deeper anatomical structures such as the periosteum and fasciae. Another kind of mechanoreceptor is located in the hypodermis, the Pacinian corpuscle, which is a bulbous structure that senses vibration. (1,2)

Skin appendages derive from the epidermis but can reach into deep layers of the dermis. They include finger nails, hairs, and different kinds of exocrine glands like the sudoriferous, sebaceous and the mammary glands. (2)

1.1.1 The extracellular matrix of the dermis

The main structural components of the dermal ECM are collagen, elastic fibres, proteoglycans and glycoproteins. These components create an extracellular network which provides the tissue with stability and defines its structure. Furthermore, the ECM

influences cell activities like proliferation, differentiation and synthesis of extracellular molecules by mechanical signalling and by regulating the bioavailability of cytokines such as TGF-β (Transforming growth factor β; see below). Fibroblasts which are not linked to the ECM usually go into apoptosis. (4)

Collagens, which make up 70% of healthy skin's dry weight, play a crucial role in determining the extracellular structure and in providing stability. (4,5) So far 28 different proteins have been discovered which can all be subsumed to the collagen family. A collagen fibre consists of three polypeptide chains, termed α-chains, which are unified to a triple helix. In some collagen fibres these α-chains are identical (homotrimers), in others they differ from each other (heterotrimers) and each of these chains consists of a repetitive sequence of three amino acids: Amino acids very commonly found in α-chains are glycine, proline and hydroxproline. By creating hydrogen bonds between different α-chains within one triple helix hydroxyproline enhances the stability of collagen strands. (4)

The biosynthesis of collagen can be divided into an intra- and an extracellular part. Intracellular post-translational processes of procollagen chains (collagen chains with C- and/or N-terminal appendages) include hydroxylation and glycosylation of amino acids, creation of disulphide bonds within and between α-chains and the folding into triple helices. After the exocytosis of the procollagen triple helix strands and the cleavage of the N- and/or C-terminal polypeptide chains the (now called) collagen strands get attached to other collagen and non-collagen fibres. (4)

Collagen fibrils (collagen triple helixes) never consist of only one type of collagen but they are a composition of different collagen proteins and are linked to other molecules like proteoglycans. The exact composition of collagen types, however, depends on where the tissue is located at and what its mechanical tasks are. However, collagen I always seems to make up the largest amount within fibrils. In the human dermis most collagens are produced by fibroblasts which create a network of ECM around themselves. (4)

The basement membrane, which represents the dermo-epidermal junction (see *Section 1.1*), mainly consists of collagen IV (this does not apply to vascular basement membranes). In order to anchor the basement membrane to the epidermis basal keratinocytes synthesise collagen XVII which inserts in the basement membrane's lamina densa (the part of the basal lamina which is rich in fibres). Hence, a strong connection between epidermis and

the basement membrane occurs. On the other side, collagen VII, mostly synthesised by fibroblasts, connects the dermal ECM to the basement membrane. (4)

Elastic fibres (1-2% of healthy skin's dry weight) are extracellular strands mainly consisting of elastin and microfibrils which have the ability to return to their original length in relaxation after being stretched by approximately 100%. (4,5)

Elastin is an amorphous and insoluble protein which is formed by cross-linking of its monomer tropoelastin and appears lucid under an electron microscope. The polypeptide chain of tropoelastin comprises repetitive sequences of hydrophobic amino acids which create cross-linking domains within the chain. Elastin molecules themselves, again, are cross-linked by desmosine, which provides these fibres with elasticity. (4)

Microfibrils mainly consist of fibrillin and form strands of 10-12nm in diameter which appear as dense structures under an electron microscope. Besides fibrillin these fibrils also contain a wide range of other proteins like microfibril-associated glycoproteins, fibulins and collagen XVI. Microfibrils are well integrated in the ECM; they represent the scaffolding of elastic fibres and regulate cell activity. One way they influence cell activity is by creating complexes together with proteoglycans which interact with TGF-β. These complexes, referred to as large latent complexes, greatly control the bioavailability of TGF-β by trapping or releasing it into the ECM. (4) When activating its receptors on the surface of fibroblasts TGF-β triggers off an intracellular cascade which ultimately leads to the transcription of its target genes, including the gene encoding for procollagen, COL1A2. Actually, the TGF-β axis is considered the main pathway to enhance collagen synthesis in dermal fibroblasts (5)

Regarding structure and composition three subtypes of elastic fibres have been defined: Oxytalan fibres, elaunin fibres and thicker fibres simply referred to as elastic fibres in a narrower sense: Bundles of parallel microfibrils anchored in the basement membrane run perpendicularly towards the depth of the skin. These "oxytalan fibres" contain very little elastin and insert into a flat network of elaunin fibres which is situated parallel to the dermo-epidermal junction. Elaunin fibres contain larger amounts of elastin and the network they form creates a link between the aforementioned oxytalan fibres and thick elastin-rich elastic fibres in the depth. Because of the different amounts of elastin in these fibre subtypes it has been hypothesised that the elastic fibres in deep layers of the reticular

dermis mainly absorb mechanical forces while more superficial fibres like oxytalan fibres serve as rigid anchorage of the basement membrane. (4,6)

One feature of elastic fibres which plays a crucial role in this thesis is that in an H&E stain and at an exciting wavelength of approximately 490nm they fluoresce much brighter than other extracellular fibres. This fluorescing feature has been ascribed to the binding characteristics between eosin and elastin rather than the composition of the elastic fibre itself. (7)

The **extrafibrillar matrix** of the connective tissue is not just a mass that fills gaps between fibres but is well organised and participates in regulatory processes and hence is being discussed in the following paragraphs (4):

Glycosaminoglycans (GAGs) are polysaccharides consisting of repetitive sequences of negatively charged disaccharides which have the ability to bind a lot of water and ions. The most common GAG is hyaluronic acid (HA) which can be found in every connective tissue. Unlike HA other GAGs commonly create covalent bonds with proteins, forming complexes referred to as proteoglycans. Proteoglycans bind to fibrillary and cellular tissue components. Some of them participate in the regulation of the structure and the mechanical features of skin by influencing fibroblasts through trapping or releasing TGF-β into the ECM (see above). The exact composition of ECM regarding GAGs and proteoglycans is highly dependent on where the tissue is located and what its tasks are. The most important proteoglycan of the dermis is called versican and generally binds to the elastic fibre system. Versican and HA create huge complexes which trap lots of water and make the skin taut. (4)

Glycoproteins mainly connect different components of the ECM with one another and hence shall briefly be mentioned: fibronectin and laminin. By forming fibrils and connecting them to both cellular and fibrous components fibronectin anchors cells like fibroblasts in the in the extracellular network of the connective tissue. Laminin interlinks fibres of the basement membrane and – via integrin – also connects fibres to cells. In this way laminin helps transmitting physical signals like mechanical tension from the ECM to the cells. (4,8)

1.2 Aging processes of the skin

There are basically two kinds of aging processes of the skin which need to be distinguished: Intrinsic and extrinsic skin aging. Intrinsic or chronological skin aging (sometimes also referred to as chronoaging) occurs in any skin with time as a result of physiological senescence of cells and tissue. Extrinsic skin aging, on the other hand, is a product of environmental influences, predominantly of long-term sun exposure and thus is also referred to as photoaging or dermatoheliosis. (9-14)

1.2.1 Intrinsic skin aging

1.2.1.1 **Clinical appearance**

Chronologically aged skin appears thin, inelastic and with fine wrinkles which, by definition, vanish when stretching the skin. (9) Other typical age-related changes include the diminution of subcutaneous fatty tissue (11) and the presence of benign neoplasms such as seborrheic keratosis and cherry angioma. (13)

Furthermore, sensory skills of the skin decline since both Pacinian and Meissner corpuscles diminish, wound healing processes become retarded due to a prolonged epidermal turnover time and epidermal vitamin D synthesis decreases. (15)

1.2.1.2 **Histological appearance**

Intrinsic skin aging is histologically characterised by a thinner epidermis due to decreased proliferation of basal keratinocytes. Along with keratinocytes Langerhans cells, melanocytes and dermal fibroblasts decrease in number. (9) The content of GAGs decreases which leads to a loss of tautness in the skin of the elderly. (13) Elastic fibres in general, but especially oxytalan fibres of the papillary dermis decrease in number and diameter while collagen fibres appear thickened, coarse and less well organised. (9-11,16)

1.2.1.3 **Pathogenesis**

The pathophysiological background of intrinsic skin aging is mostly ascribed to physiological cell senescence leading to decreased productivity and proliferation. (9)

Compared to young cells, aged dermal fibroblasts were observed to be far more often in the G_0 and G_1 phases of the cell cycle and less frequent in the G_2, M and S phases. Many genes involved in cell cycle progression were found to be downregulated whereas genes

which interrupt the cell cycle, such as p16 and p21, were upregulated. Furthermore, it has been suggested that the length of telomeres itself could have an influence on the cell cycle and the expression of genes. As a result of past cell divisions this length physiologically decreases with time and hence there is a strong inverse correlation between cell age and telomere length. (5)

More evidence for decreased cell activity is provided by the fact that all of the proteins involved in the collagen synthesising TGF-β signalling axis are decreased in senescent fibroblasts. (5)

As described in *Section 1.2.2.3*, reactive oxygen species (ROS) play a major role in the pathogenesis of extrinsic skin aging. To a lesser degree they also contribute to the pathogenesis of chronoaging: Along with the antioxidant capacity of aged fibroblasts, the elimination of ROS physiologically produced in the respiratory chain in mitochondria decreases. These ROS alter the structure and skills of proteins, lipids and DNA leading to reduced efficiency of fibroblasts. (5)

1.2.2 Extrinsic skin aging

Since the degree of photoaging correlates with the amount of sunlight the skin has been exposed to it develops and increases with time. Hence, extrinsic skin aging develops simultaneously with intrinsic skin aging in sun exposed areas and its manifestation can unexceptionally be seen along with age-related skin alterations. (15)

The main risk factor for the development of dermatoheliosis is fair skin which does not tan (see *Section 1.2.2.1*). (12,14) Besides cumulative solar irradiation, environmental factors contributing to photoaging are smoking and to a lesser degree air pollution. (12,13,17) Photoaged skin, of course, is also associated with a series of other sun-related diseases such as actinic keratosis, basal cell carcinoma (BCC) and squamous cell carcinoma (SCC). (13)

1.2.2.1 **Clinical appearance and ethnic-specific features**

The most prominent feature of photoaging is the appearance of deep and thickened (sometimes ever referred to as furrowed) wrinkles which, unlike wrinkles in chronoaged skin, do not disappear when stretching the skin. Moreover, the skin becomes coarse, leathery, dry, and inelastic. It often appears in a yellow hue and develops telangiectasia as well as pigment alterations such as solar lentigines. (9,12,14) Photoaged skin loses its

physical resilience and lacks immunological competence making it highly vulnerable to mechanical forces and prone to chronic infections. (12,14)

Solar elastosis as the most prominent histological correlate of photoaged skin (see *Section 1.2.2.2*) appears in a number of separately defined entities which can all be subsumed under the designation “solar elastotic syndromes”. (15) One entity of this group is called cutis rhomboidalis nuchae and appears as vastly thickened, leathery skin at the neck with furrowed wrinkles that seemingly intersect the skin into geometric shapes. The Favre-Racouchot Syndrome, to name another solar elastotitc syndrome, appears along with dermal cysts and open comedones, it depicts the same coarse wrinkles as described at the beginning of this section and is typically seen in facial skin. (9,12,15,16,18)

In contrast to intrinsic skin aging, extrinsic skin aging varies substantially in its onset and the extent of its morphological appearance between individuals and especially between ethnical groups. Apart from the environmental factors mentioned in *Section 1.2.2*, genetically determined characteristics greatly influence the occurrence of photoaging. Composition and amount of skin pigmentation seem to represent the most important individual features to have an effect on the development of photoaging, whereby fair skin, Fitzpatrick Skin Type I in particular but also Type II, has the highest risk. (17,19) Photoaging in darker skin of people from South Asia or Africa is less common, generally has a significantly later onset and comes along with milder changes. These changes mainly include seborrheic keratosis, fine wrinkling and pigmentation alterations. (18)

Compared to Europeans Japanese females exhibit less severe wrinkles in photoaged skin which is ascribed to higher levels of antioxidants in their bloods. Hence, systemic factors seem to play a role in the development of extrinsic skin aging too. (17)

1.2.2.2 **Histological appearance**

Similarly to changes of chronologically aged skin the epidermis mostly appears thinner but can also depict mild acanthosis. (9,10) The wavy course of the dermo-epidermal junction flattens and the dermal papillae become shorter. (13) Epidermal melanin contents appear inhomogeneously distributed among keratinocytes leading to macroscopically irregular alternations between hyper- and hypopigmentation. (11,14) The number of Langerhans cells in photoaged skin is even lower than in chronologically aged skin. (14)

The most obvious histological feature of photoaged skin is called solar elastosis, it generally fulfils the staining criteria of elastic tissue and probably mainly derives from elastic fibres (hence the designation solar/actinic elastosis). Accordingly, in H&E stained tissue sections it appears as a faintly basophilic, fibrillary entity (see *Figure 1* below). (9,11,13-15) Solar elastosis is obligatory found in skin with chronic sun damage (CSD) and can be diagnosed histologically long before photoaging becomes clinically apparent. Initially it accumulates in the lower papillary dermis before it expands into deeper dermal layers, always sparing a narrow band of seemingly unaltered connective tissue right beneath the dermo-epidermal junction. This band is referred to as "grenz zone" and mainly consists of dense collagen fibres. (9,11,14,15)

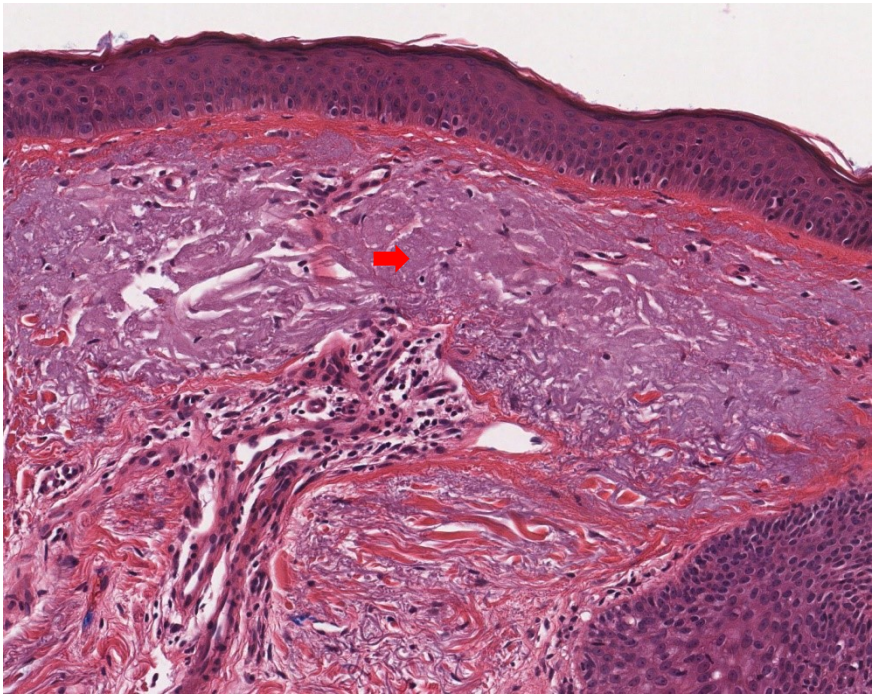

Figure 1: Bright-field microscopic appearance of advanced solar elastosis in an H&E stained skin tissue sample (×170)
Skin sample obtained from the face of a 60 year old male patient. The *red arrow* points at faintly basophilic amorphous advanced solar elastosis. Also note the flattened dermo-epidermal junction and the narrow grenz zone containing no basophilic fibres.

Solar elastosis consists of abnormal elastic tissue with a minor collagenous component and forms thickened fibrous structures which can merge to huge amorphous masses in advanced cases. (9,11,14,16,18) Histochemical analyses have shown that it mainly contains elastin, fibronectin and little amounts of collagens and that it is sensitive to elastase, corresponding with the assumption that it derives from the elastic fibre system. (9,11,16) The few collagen fibres remaining in photoaged skin are thinner than in healthy skin and sometimes split up into their fibrils towards their ends. (9,11)

Electron microscopic images of solar elastosis depict increased amounts of granular elastin which create inhomogeneous masses around extraordinarily electron-dense microfibrils. Some elastic fibres depict disrupted sections and show granular residues which sometimes appear in “moth-eaten”-like shapes. (11,14)

Alterations of versican along with a decreased ability of HA to bind water have been reported, giving one histological correlate for the loss of tautness in photoaged skin. (20)

As mentioned in *Section 1.1.1* elastic fibres can be distinguished from other extracellular components in H&E stained tissue samples by their strong autofluorescent activity when excited at a wavelength of approximately 490nm. In *Characterizing cutaneous elastic fibers by eosin fluorescence detected by fluorescence microscopy* Heo and colleagues (7) described for the first time that this feature ceases in in photoaged skin.

The specimens included in this thesis have been evaluated by three collaborating dermatopathologists from Queensland, Australia. Evaluating H&E stained slides they have subjectively assigned the extent of solar elastosis in each specimen to one of four semiquantitative categories: “nil”, “mild”, “moderate” or “marked”. Specimens categorised as “mild” presented with a mildly increased number of elastic fibres within the papillary dermis. These fibres were structurally identical with or slightly thicker than normal elastic fibres. Specimens were labelled as “moderate” or “marked” if vast elastotic changes were apparent: numerous enlarged, tortuous basophilic fibres situated in the papillary as well as the reticular dermis, sometimes merging into large amorphous elastotic masses. However, due to various non-specified reasons some of the slides could not be evaluated and were hence assigned to a separate class “(not classified)”. (21)

1.2.2.3 **Pathogenesis**

Chronic exposure to sunlight is unequivocally the most important environmental cause of extrinsic skin aging, its exact pathogenesis, however, is still a matter of debate. In this section I will describe current considerations and hypotheses:

First of all, we need to specify which fractions of sunlight play a role in extrinsic skin aging: The ultraviolet (UV), as well as the infrared A (IRA, 770-1400nm) fractions of solar radiation have been discovered to cause a series of processes in the skin which may all contribute to the development of photoaging. In this context, two subclasses of the rather large spectrum of UV light need to be specified: one fraction which covers wavelengths just too short for a human eye’s perception (UVA, 320-400nm) and another fraction of

higher frequencies (UVB, 290-320nm). (17) In literature other subclasses of the UV light, the frequencies of which are situated between the ones of visual light and X-radiation (22), do not get mentioned in the context of photoaging. Higher frequencies do not penetrate far into the depth of the skin which might give an answer to why they do not play a role in photoaging.

The emergence of ROS plays a central role in extrinsic skin aging and triggers off a series of dermal reactions. There are a number of environmental factors which lead to the genesis of ROS and are associated with extrinsic skin aging: UV light (more specifically UVA and UVB) probably leads to the largest portion of dermal ROS genesis. IRA mainly induces ROS in mitochondria since this is where its frequencies are mainly absorbed. Apart from radiation, smoking and air pollution also induce ROS. It has been suggested that airborne particulate matter can generate ROS both as an immediate response and via carrying organic chemicals and metals which diffuse to dermal mitochondria. (17)

ROS can stimulate cytokine- and growth factor-receptors on the surface of both fibroblasts and keratinocytes. This stimulation triggers off an intracellular cascade which ultimately leads to elevated transcriptions of NFκB and activating protein 1 (AP-1). NFκB increases the expression of proinflammatory cytokines which attract neutrophils and stimulate them to release enzymes like the neutrophil collagenase and the neutrophil elastase. Elevated intracellular AP-1 levels, on the other hand, decrease the expression of collagen I and III and at the same time increase the expression of certain endopeptidases, called matrix metalloproteinases (MMPs). (5,12,14,17)

The family of MMPs is generally known to degrade extracellular collagens, elastin, and proteoglycans. Recent investigations, however, question the immediate role of MMPs in tissue degradation and emphasise their role in triggering inflammatory processes: MMPs influence intracellular processes resulting in activation of chemokines and cytokines such as tumour necrosis factors and hence support inflammation and attraction of neutrophils. (23) A documented increment of T cells and dendritic cells after solar irradiation in areas of solar elastosis further confirm the assumption that inflammation could play a crucial pathogenetic role. (14)

An association between solar elastosis and neutrophil elastase was demonstrated in murine models. This observation corresponds to the general consensus that solar elastosis primarily results from alterations in the elastic fibre system rather than the collagen system

and emphasises the role of inflammation and neutrophils in the pathogenesis of solar elastosis. (23)

Furthermore, PKCδ (protein kinase C, isoform δ) was suggested to participate in the same processes: PKCδ is an intracellular enzyme located in the cytoplasm which, when translocating to the nucleus, can activate a series of transcription factors, including NFκB and AP-1 (see above). Investigations using UVA-induced genesis of ROS showed PKCδ translocation to the nucleus suggesting an important role for PKCδ in cellular responses to elevated ROS levels. (24)

The physiological genesis of ROS within mitochondria during the process of ATP synthesis in the respiratory chain can be elevated to a multiple of the normal level by continuous UVA irradiation. The limited capacity of mitochondrial DNA repair mechanisms cannot cope with vastly elevated ROS levels as in UVA-exposed skin areas, leading to mutations of the mitochondrial DNA (mtDNA). Furthermore, UVR can also cause immediate damage to mtDNA. However, these mutations are associated with increased MMP-1 levels, leaving us with another causal link between ROS emergence and inflammation. (17) (9,14)

Another feature of ROS is that they can oxidise amino acids and thereby alter protein structures, resulting in impaired enzymatic features. Consequently, the ability of proteasomes to successfully degrade aged fibres of the ECM is compromised. Apart from that, a high portion of oxidised extracellular proteins was found in regions of solar elastosis, suggesting immediate protein alterations due to ROS in the ECM. (9,17,25) Furthermore, UVR-induced ROS were shown to create N^{ε}-(carboxymethyl)lysine (CML) in the dermis, a major compound assigned to the group of advanced glycation end products (AGEs). The presence of CML was demonstrated to prevent elastin from degradation by elastases and thereby could contribute to accumulation of elastotic material. (26)

Electron-microscopic evaluations of regions with solar elastosis have shown fibroblasts which synthesise and excrete granular material. (11) Furthermore, ROS-induced elevated promoter activity and mRNA levels of elastin were found in elastotic lesions, suggesting the assumption that newly synthesised abnormal elastin could also play a role in the genesis of solar elastosis. (27) Hence, accumulation of solar elastosis may result from both decreased susceptibility to enzymatic degradation and increased synthesis. (26)

Fibroblasts in solar irradiated skin exhibit a fewer TGF-β type II receptors and appear less firmly anchored in the ECM due to degenerative processes of the tissue. These conditions decrease the fibroblasts' sensitivity to biochemical and mechanical stimuli from their immediate surrounding. (5,9)

To summarise, the emergence of ROS unequivocally plays a central role and marks the origin of a series of consequent intra- and extracellular reactions and processes. The fact that Japanese women develop only mildly photoaged skin because of their elevated antioxidant levels (see *Section 1.2.2.1*) provides a clinical indication for the pathogenetic role of ROS. ROS directly and mediated through responses of the tissue induce inflammation which damages both intra- and extracellular structures and processes ultimately resulting in an imbalance between synthesis and degradation of abnormal ECM.

A series of processes have been discovered which can contribute to the emergence of solar elastosis. However, an ultimate and conclusive pathogenetic explanation for the development of extrinsic skin aging could still not be established.

1.2.2.4 **Preventative measures and therapeutical approaches**

Any preventative measure that minimises solar irradiation onto skin like the usage of sun screen or avoidance of direct sunlight and smoking significantly reduces the occurrence of solar elastosis. Therapeutical approaches which are initiated after its occurrence cannot compensate any failure to prevent it. (12,14,16)

Topical application of moisturising creams can strengthen the skin's resilience against mechanical forces and decrease the risk of superficial injuries. The changes of dermatoheliosis have been discovered to improve after the topical application of vitamin A and retinoid derivates, immunosuppressive drugs like tacrolimus and after injections of hyaluronic acid. Other approaches include light, laser and surgical therapies as well as chemical peelings. (12,14,16)

1.3 Malignant melanoma

The specimens used in this study are samples of human cutaneous malignant melanoma (MM). The MM is a malignant tumour which derives from melanocytes and as such is most commonly seen on the skin. Besides the skin it can also occur on mucous membranes, the gastro-intestinal system, the eye and the central nervous system. The MM is the third most common malignant tumour of the skin next to BCC and the SCC. (1)

1.3.1 Subtypes

There are a few subtypes of cutaneous MMs, the most common ones of which should be differentiated especially since their pathogenesis is not uniform:

The **superficial spreading melanoma** (SSM) makes up about 57% (1) of all MMs and is characterised by a primarily horizontal pattern of infiltration. Atypical melanocytes can be found in every layer of the epidermis. (28)

The **nodular melanoma** (NM) is the second most common MM (21% (1)) and typically appears as a prominent, mostly but not always pigmented node with distinct boundaries. (28)

The **lentigo maligna melanoma** (LMM) is the only subtype that arises due to chronic sun exposure (see *Section 1.3.2*) via a carcinoma in situ, referred to as lentigo maligna. Initially the melanocytes strictly infiltrate horizontally at the level of basal keratinocytes and at superficial parts of hair follicles. (28)

The **acral lentiginous** and the **mucosal melanomas** appear on hairless skin and on mucous membranes respectively. These subtypes of MMs are not considered to emerge due to solar irradiation and hence will not be discussed any further in the following sections. (28)

1.3.2 Epidemiology, aetiology and pathogenesis

The incidence of MMs has recently increased: during the last couple of decades it has risen by 4 to 6% per year. The MM is primarily a disease of the fair-skinned Caucasian and very rarely occurs in countries with predominantly ethnical groups of darker skin. Its highest incidence rate is found in Australia (39/100,000 per year); in Europe it is around 4-10/100,000 per year. The incidence is also clearly dependent from the latitude with an increment closer to the equator. Interestingly, women are more likely than men to develop a MM at high latitudes and vice versa at low latitudes. (29)

The MM hardly ever occurs before the 4^{th} decade of life, after that becomes more common and finally peaks at the 7^{th} to 8^{th} decade. In total numbers it most commonly occurs on the body's trunk, men predominantly develop them on their backs and shoulders while women tend to develop them on their lower limbs. However, in relation to the surface area the most common location for MMs is the face. (29)

Risk factors for the MM are a series of familial genetic aberrations, dysplastic naevi (naevi consist of benign proliferations of melanocytes), fair skin, a past medical history of skin cancers other than MM and xeroderma pigmentosum (a disease in which the lack of DNA repair mechanisms leads to destruction of cells, tissue and organs (1)). The only assured environmental risk factor is sunlight; sunburns especially during the childhood seem to represent a particular risk but how exactly and under which conditions solar irradiation effects the development of MMs is not entirely clear. (28)

There is much evidence that the association between solar irradiation and the emergence of keratinocyte-based skin tumours like the SCC is rather linear. In other words, chronic solar irradiation is the primary cause for SCCs. This does not apply to the pathogenesis MMs: the influence of ultraviolet radiation on its tumorigenesis is complex, depends on the subtype of melanoma and still is not entirely clarified. (28)

UV light covers a spectrum of solar radiation which is energetically higher than visible light (for subclasses of UVR see *Section 1.2.2.3*). The ratio of UVA/UVB light that reaches the surface of the earth depends on a series of parameters such as weather conditions and altitude. One aforementioned epidemiologically important parameter which lowers the portion of UVB light is increased latitude. An association between MMs and UVA light has been suggested because the incidence of MMs does not decrease as drastically with increased latitude as the incidence of SCCs which is unequivocally associated to UVB light. (28)

Furthermore, for the development of SCCs a strong correlation with CSD is well documented. A MM, however, is more likely to emerge on skin with intermittent exposure to UVR, as it is more common among indoor than outdoor workers and in total number it is seen more often on the trunk than on the head or the neck. (28)

In 2003 a so called “divergent pathway” to explain the heterogeneity in melanoma development has been established which differentiates between MMs arising from CSD and those which do not (28):

The **CSD pathway** is typically histologically associated with the presence of solar elastosis as a marker of CSD (see *Section 1.2.2.2*) and is usually found in skin of patients with only a few naevi. They generally have a later onset (7^{th} to 8^{th} decade (29)) and mostly develop on the head or the neck. The LMM is the only subtype that is strictly associated with the CSD pathway. (28)

The second pathway, also referred to as **non-CSD pathway**, results in an earlier onset of the tumour (5^{th} to 6^{th} decade (29)), is mostly found on body regions with intermittent rather than chronic sun exposure such as the trunk and is associated with patients who have a lot of naevi. Interestingly most naevi carry mutations of the signal protein BRAF which is considered a proto-oncogene. (28,30) These BRAF mutations (the most common mutation is $BRAF^{V600E}$) can probably be considered an early event of melanoma development but does not provide entire transformation to malignancy. However, since the non-CSD pathway is associated with high counts of naevi and naevi often carry BRAF mutation it has been suggested that there could also be an association between the non-CSD pathway and BRAF mutations which actually turned out to be true. In fact, nowadays BRAF mutations are considered the most reliable marker for the non-CSD pathway of MMs. (28)

It should be mentioned that the overwhelming majority of MMs in total number (see above) seem to arise from the non-CSD pathway. (28)

Many observations about how UVR effects the behaviour of melanocytes have been made, including increased synthesis of cytokines like α-MSH and ACTH which increase melanocytic proliferation, decreased activity of the immune system, inflammation, immediate DNA damage and many more. If and to which extent these phenomena participate in the pathophysiological mechanisms involved in the genesis of MMs could not be clarified to date. (28)

1.3.3 Diagnosis, prognosis and therapy

The diagnosis of a MM is usually made by inspection using a dermatoscope to visually enlarge the lesion of interest. The lesion is then assessed using four criteria which can easily be remembered by the acronym ABCD. Signs of malignancy according to this rule are:

- **A**symmetry of both shape and colour
- **B**order irregularities and difficulty to exactly circumscribe the tumour
- **C**olour inhomogeneity: the more colours can be found the more likely the lesion is malignant
- **D**ynamics: fast progression of growth, changes in colour, thickness, surface structure, etc. (31)

Originally D was defined as diameter and indicated malignancy if greater than 5mm. Since early diagnoses have become more frequent and are of great importance this criterion was changed to dynamics in 2005. In some cases the dynamics may be the only feature of a lesion that leads to a diagnosis: Especially NMs often lack abnormality in features A-C. (31)

If a potentially malignant lesion is found it gets surgically removed and histologically assessed. (1) If the histological appearance does not rule out other carcinomas or sarcomas the tissue becomes immunohistologically assessed which mostly allows a doubtless diagnosis. (31)

The American Joint Committee on Cancer (AJCC) has established a staging system for malignant tumours which defines the individual prognosis and affects consequent therapeutical procedures. First, a series of measurements which create the so-called TNM-classification need to be taken which gauge the progression of a MM:

- The **T** component summarises the depth of infiltration, the mitotic rate of the tumour and the presence of ulcerations. The depth of infiltration is measured in mm and is also referred to as Breslow's index.
- **N** provides information about the infiltration of regional lymph nodes. It summarises how many lymph nodes are affected and how heavily they have been metastasised into (mircometastases or macrometastases).
- Finally the **M** component consists of information regarding the presence and location of distant metastases and the level of the serum lactate dehydrogenase. (31)

All these measurements are combined to create the TNM-classification which then can be used to determine the stage of the tumour. Depending on this tumour stage the individual prognosis varies drastically ranging from a life expectancy of about a year if lung metastases are present to a five-year-survival-rate of more than 90% if the Breslow's depth is lower than 1mm and no ulcerations are present. (31) Early diagnosis is extremely important since the outcome at the mostly initial radial infiltration phase is extremely good and declines as the tumour infiltrates vertically. After all, MMs are responsible for 90% of death cases of all malignant skin tumours due to their early propensity to metastatic spread. (1,31)

As aforementioned the primary lesion gets removed via surgical excision for diagnostic purposes. Depending on the histological evaluation and tumour staging another, therapeutical excision at the same location in order to create a larger distance to the macroscopically visual margins might be indicated. Since MMs have been proven to be sensitive to radiation, radiotherapy can be indicated symptomatically for the treatment of distant metastases in the brain or the bones and as an adjuvant approach for primary lesions. Schemes for topical and systemic drug therapy including immunotherapy, immunomodulation and chemotherapy have been established and are generally not curative but mostly intend to remedy symptoms or to prolong relapse-free periods. (1,32)

1.4 Context and leading question

The example of malignant melanoma, which two main pathogenetic pathways have been established for, highlights the fact that the exact impact of solar radiation on the genesis of some dermatologic diseases has still not been entirely clarified. A standardised procedure which can objectively quantify the degree of accumulated solar irradiation on human skin could be a useful tool for epidemiological studies. The extent of accumulated solar irradiation as an environmental risk factor could be determined, not only for malignant melanomas but for a series of dermatological conditions.

The current research approach to estimate the degree of accumulated solar irradiation on skin regions is usually a semiquantitative one and depends on the experience and the subjective perception of the evaluating pathologist. In this thesis I have established two independent histological approaches to gauge the accumulated impact of solar radiation on human skin and have tested the accuracy of these methods:

- Using a colour-based computer program I have sought to objectively quantify the amount of matter with the staining characterictics of elastic fibres within a predefined range of dermal skin tissue. Within this range the computer program has calculated the portion of pixels covering tissue stained positively for elastic fibres. For practicability reasons I will refer to this method as the “Positivity-Method” (PM).
- H&E stained elastic fibres generally display very high autofluorescent activity when excited at a wavelength of 490nm (see *Section 1.1.1*). This activity has been discovered to decrease in skin tissue frequently exposed to UVR (see *Section 1.2.2.2*). Since elastic fibres in superficial dermal layers are certainly more exposed

to UVR than in deeper layers, the autofluorescent activity will first decline in fibres situated closely to the surface. In other words, the deeper one need to go to find fluorescing elastic fibres, the higher the degree of solar irradiation onto this skin spot has to have been. Based on this consideration, the second method established has sought to conclude the degree of sun exposure from the depth of the most superficial autofluorescent elastic fibres. In the following I am going to refer to this method as the "Loss of Fluorescence-Method" (LoFM).

These two methods have been tested by comparing them with the subjective evaluation of dermatopathologists who had assigned the samples to four quantitative categories of solar elastosis ("nil", "mild", "moderate" and "marked") as described in *Section 1.2.2.2*. Furthermore, I have examined the correlation between the two methods.

2 Patients und Methods

For my investigation at the QIMR Berghofer Medical Research Institute in Brisbane, Australia I used excisional skin samples containing melanoma tissue and adjacent non-tumorous skin of 55 patients (one biopsy of each patient) who had all been diagnosed with different types of malignant melanoma. A brief overview of the patients' characteristics, including age, sex and melanoma subtypes is listed in *Table 1*.

The skin samples had all been collected and processed in Australia. I conducted my investigation in melanoma skin samples because the results of my thesis were intended to be used in further epidemiological investigations revolving around the different pathways of malignant melanoma.

The following chapter describes preparation techniques of the histological slides, image acquisition, evaluation and statistical approaches I have used in order to test my methods (see *Section 1.4*).

sex	no. of patients	**age range in years**	no. of patients	**melanoma subtype**	no. of patients
male	42	**18-39**	7	**SSM**	40
female	13	**40-59**	18	**LMM**	7
Total	55	**60-79**	30	**NM**	4
		Total	55	**Not specified**	4
				Total	55

Table 1: Overview of patients' distribution regarding age, sex and melanoma subtype

2.1 Pre-staining Preparations

Before being able to apply histological stains to the specimens there are a series of steps which need to be conducted in order to place thin tissue ribbons onto microscopic glass slides. These steps aim to preserve the samples from degradation due to microorganisms, stabilise their histological structures and create smooth wax blocks which can then be cut into evenly thick tissue ribbons. (33-35)

Fixation

The fixation is the first step of preparation a biopsy needs to pass through. Because of its antimicrobial effects it kills cells and microorganisms and therefore preserves the tissue from any misleading alterations. It reassures that the histological structures and the cellular components are all kept in place by creating covalent bonds between amino acids and nucleic acids. Furthermore, the fixative is also said to increase the tissue's affinity to histological dyes applied later on and hence increases the optical contrast between different tissue components. (33-35)

In order to avoid structural alterations of the slides it is necessary not to use tissue pieces which are too bulky to be entirely penetrated by the fixative. These bulky pieces would lose their unfixed central regions during the process of sectioning. It is important to leave the specimens in the fixative solution for the recommended period of time. If this time is exceeded, the so-called "overfixed" tissue samples will become quite hard and therefore complicate the sectioning process. On the other hand, if the fixation time is too short the "underfixed" sample might be exposed to putrefaction due to a loss of the fixative's antimicrobial effect. (33)

All of the specimens used in this thesis were treated with formalin. Formalin is a hydrophilic liquid and is assigned to the group of non-coagulating fixatives. In contrast to coagulating fixatives, this group of substances does not lead to alterations of the secondary and tertiary structures of proteins but actually preserves them. This feature is of special interest in immunohistochemistry which is not used in this thesis. However, since this fixative does not do any extra harm to the histological structures it was applied to the specimends of this thesis. Other advantages of formalin include that it is inexpensive and easy to acquire. (33)

On the other hand, vaporised formalin is potentially carcinogenic and therefore should be treated with caution. Long-term exposure to air can lower the pH of formalin and should hence be avoided. Its pH should stay in a rather narrow range in order to preserve its chemical features. If the solution becomes too acidic major alterations like areas of black pigment may occur in the treated tissue sections. Dramatic alterations of tissue, however, can be avoided by thorough handling. (33)

Formalin is a solution of 37-40% formaldehyde. A 1:10 dilution of this solution becomes applied to the specimens, creating a 3.7-4% solution of formaldehyde for tissue treatment. (33)

Embedding

Since the specimens need to be cut into even ribbons of only a few micrometres in thickness and they are quite fragile after fixation, they need to be embedded in a substance which equally penetrates it, fills up gaps which might occur due to dehydration, does not chemically or physically interact with it and stabilizes its histological structure. The most common substance used for this purpose is paraffin. (33,35) All of the specimens used in this thesis have been treated with paraffin.

Paraffin is hydrophobic while formalin is an aqueous fixative. Hence, putting the freshly fixed tissue into a chamber of paraffin would never actually embed the sample. The water trapped in the specimen needs to be exchanged by a series of ethanol solutions with increasing concentration. After that ethanol needs to be replaced by a substance termed clearing agent which, again, can be replaced by paraffin. The clearing agent applied to the samples in this thesis was xylene which is inexpensive and widely used. Its fumes are toxic and hence it requires to be used with caution. (2,33)

After being treated with xylene, the specimen is ready to be infiltrated with paraffin. The tissue piece becomes both infiltrated and surrounded by paraffin so that it ends up in a cube- or cuboid-shaped block of wax. This block of wax allows smooth and even sectioning and provides the histotechnician with some kind of orientation within the samples. During the process of mounting this orientation makes it easier to let different slices of one specimen face the same direction in each slide. This simplifies the comparative observation of slides deriving from the same specimen. Formalin fixed, paraffin embedded (FFPE) specimens as created here represent a very common approach of tissue preparation. (33)

Sectioning

The process of cutting histological specimens into thin tissue ribbons of a few or only one layer of cells is termed sectioning. When looking at a tissue ribbon through a bright-field microscope the ability to see small details will cease with the number of cells the light has to pass through. Accordingly, any histological details will be harder to identify with increased tissue thickness. (33-35)

For the PM the thickness of the sections should be kept low in order to avoid the phenomenon that elastotic and non-elastotic extracellular components overlap which would complicate the process of elastosis quantification. Regarding the LoFM, increased tissue thickness would enhance the autofluorescence of non-elastic fibres. In this case healthy elastic fibres would need to fluoresce much brighter in order to allow differentiation between them and other extracellular components. That would make the detection of thin healthy elastic fibres by fluorescence microscopy less sensitive. As we can see, in theory both methodological approaches should be supported by setting the tissue thickness low. At the same time it is important to secure the section's integrity. Very thin sections might rip apart while being sectioned or mounted. (33)

Because of the considerations discussed above all of the specimens included in my investigations were cut at a thickness of 4µm.

Mounting onto microscopic slides

Freshly cut sections get removed from the microtome and transferred into a water bath using a wooden stick or a spatula. The water bath should be 5-10°C cooler than the melting point of paraffin. If the water is too warm the wax ribbons can dissolve in the bath, if it is too cool the ribbons can shrink and develop wrinkles. Bonding agents like albumin, Elmer's Glue or poly-L-lysine can be added to the water in order to increase the adhesion between microscopic slide and tissue ribbon. (33)

The tissue ribbons used for both methods were mounted onto X-tra® Slides which have a positively charged surface and therefore improve the adhesion between slide and tissue. Using these slides, bonding agents were not required to be added to the water bath, the temperature of which was set between 45°C and 50°C. (36)

Another crucial step is not to leave the wax tissue in the bath for more than one or two minutes. Otherwise the tissue would overhydrate, swell and appear oedematous. The water bath needs to be skimmed regularly in order to clear it from any tissue pieces that become liberated from the ribbons. These pieces, referred to as "floaters", could adhere to ribbons other than they originated from, mixing tissue parts from different specimens. Hence, the water bath needs to be maintained regularly. (33)

In a next step, the tissue ribbons simply become attached to microscopic slides by fishing them out of the bath using the slides. (33)

2.2 Staining

Since tissue itself does not appear in any colour and consequently one would not be able to identify most of the histological components the process of staining is needed to make assessing specimens even possible. Single staining solutions usually differ in colour and affinity to molecular features of tissue. This affinity is mostly based on electrostatic interactions between the stain and tissue components. (2)

In order to get the slides ready for the application of stains a few more steps need to be conducted:

First of all, the slides need to be put into an oven at 56°C for at least one hour in order to properly stick together with the tissue ribbons mounted. The slides are then dipped into xylene in order to remove the previously applied paraffin from the tissue ribbons. This step is necessary since the slides need to get rehydrated in order to subsequently be able to be penetrated by aqueous staining solutions. Rehydration is accomplished by a series of ethanol solutions with decreasing concentration. (33)

2.2.1 H&E

Hematoxylin and eosin (H&E) represent one of the most frequently used combinations of stains. Hematein – the oxidation product of hematoxylin – is a blue dye and creates a complex bond with a cation (Al^{3+}, Fe^{3+}, Cr^{3+}) which binds to acidic tissue components. Eosin, on the other hand, is a red and acidic stain and binds to basic molecules. Consequently, the histological designation for tissue which stains with hematoxylin is basophilic, whilst structures which stain with eosin are referred to as eosinophilic. (2)

Typical staining patterns of H&E are:

- Nuclei: blue
- Cytoplasm: red, bluish if it contains a lot of ribosomes
- Collagen fibres: red
- Elastic fibres: pale red or unstained (2)

The staining procedure was carried out by the Leica ST5010-CV5030 Workstation which consists of the Leica ST5010 Autostainer XL and the Leica CV5030 Coverslipper.

The Leica ST5010 Autostainer XL uses racks provided with 15 slots for histological slides and precisely follows staining protocols which can be manually adjusted or entirely newly

programmed for specific requirements. The autostainer simply moves the racks from one pot filled staining solution to another. In case the autostainer completes the entire staining procedure the rack can automatically be transferred to the Leica CV5030 Coverslipper which consequently mounts a glass cover on top of the tissue ribbon (see below). (37)

The following staining protocol includes steps of deparaffinisation and rehydration and continues with the specimen preparation after having them mounted onto glass slides:

- Xylene (3 pots, 1min each)
- Absolute ethanol (2 pots, 1min each)
- 90% ethanol (2min)
- 70% ethanol (2min)
- Running tap water (5min)
- Mayer's haematoxylin stain (see below; 7min)
- Running tap water (5min)
- Scott's tap water substitute (magnesium chloride infused water; quick rinse)
- Running tap water (5min)
- 90% ethanol (quick dip)
- Alcoholic eosin solution (HCl precipitated Eosin Y) (4min)
- Absolute ethanol (4 pots, up to 2min each)
- Xylene (2 pots, 1min each)

(This is the standard protocol for H&E stains at the QIMR Berghofer Medical Research Institute)

Mayer's haematoxylin stain is one of many solutions which all contain haematoxylin crystals and which all are similar to each other. As mentioned above, haematoxylin is a solution which requires a cation for its staining characteristics; Mayer's haematoxylin uses aluminium for this purpose. There are also a series of slightly different eosin solutions which I do not want to go into further detail about (here "HCl precipitated Eosin Y" was applied). (38)

After passing through all the pots listed above the slides were moved over to the Leica CV5030 Coverslipper (see *Section 2.3*).

2.2.2 Orcein Elastin Stain (OES)

To selectively stain elastic fibres and make it as easy as possible for a colour-based computer analysis program to quantify its portion within tissue areas I decided to use the Orcein Technique which was introduced by Unna in 1891 and dyes elastic tissue in a dark brownish hue. This technique and brown stains in general do not get applied very frequently anymore since brown hues can be confounded with artefacts which often also appear in a brown colour. However, I still decided to apply this technique to the slides because it has a simple protocol and its solution has an extremely high selectivity for elastic tissue. Furthermore, it can easily be differentiated from the counterstain applied to the same slides (see below) which provides good preconditions for the consequent colour-based computer analysis. It is important to mention that this stain does not allow differentiation between healthy elastic fibres and elastotic tissue. In the following I am going to refer to this stain as Orcein Elastin Stain (OES) (39)

The exact mechanism of how orcein binds to elastin is not clear. Van der Waals forces are being considered to play a role in the molecular binding process. (39)

If a section contains a lot of melanin and the primary interest of the observation is not melanin itself but other extracellular structures as in the PM, it makes sense to get rid of the pigmentation. Extensive amounts of melanin can both mask histological structures of interest and interfere with the staining process. (33) As mentioned above, Unna's OES appears in a brown hue. The quantification of elastic fibres was conducted by a computer program which operated by detecting different colours within predefined regions (see *Section 2.5.1.1*). Hence, the analysis program could recognise melanin as histological structures stained with OES. Because of these considerations, I decided to clear all the specimens of the PM from melanin before staining them with OES.

The protocol for the melanin bleach was applied to slides which had just been mounted with FFPE specimens and dried at 56°C:

- Xylene (3 pots, 1min each)
- Absolute ethanol (2 pots, 1min each)
- 90% ethanol (2min)
- 70% ethanol (2min)
- Running tap water (5min)
- Distilled water (quick rinse)

- 0.25% aqueous potassium permanganate (~45min)
- Running tap water (5min)
- 5% aqueous oxalic acid (until sections are macroscopically cleared from melanin; 2-5min)
- Running tap water (10min) (38)

Since potassium permanganate can react quite aggressively with tissue sections alterations can occur, however, none were noticed in the slides tested as part of this thesis. (38)

After having cleared the specimens from melanin the slides were stained with OES. Since this stain selectively dyes elastic fibres a counterstain was required to be applied. Counterstains are used to visualise a wide range of tissue components and to hence enable the observer to orientate themselves within the slides. The exact location of tissue components such as elastic fibres can only be done with an adequate counterstain.

Glynn Rees, Senior Scientific and Technical Officer at the QIMR's HistoTechnology Facility applied a counterstain called Light Green which provided a blue-greenish hue with a special affinity to extracellular components like collagen fibres (see *Figure 2* below). This dye is usually applied as a counterstain for other stains like Grocott's Method for Fungi (GMS) (38,40) but Glynn Rees adopted it for the OES (Light Green as a counterstain for OES has never been published). A major advantage of this counterstain is that a colour-based computer program can easily differentiate this counterstain's blue-greenish hue from the dark brownish hue of the OES which I was trying to quantify.

In order to prepare the orcein solution 1g of orcein was dissolved in 100ml of 70% ethanol at a gently increased temperature. Afterwards 1g of HCl was added to the cooled solution. Furthermore, 1% of acid-alcohol was prepared by adding 1ml of concentrated HCl to 99ml of 70% ethanol. This second solution's effect is to clear the specimen from excessive dye later on. (39)

For the staining procedure the slides were taken to pots containing the following liquids:

- 70% ethanol
- Orcein solution (2h)
- Rinse in 70% ethanol
- 1% acid-alcohol (2min)
- Running tap water (5min) (39)

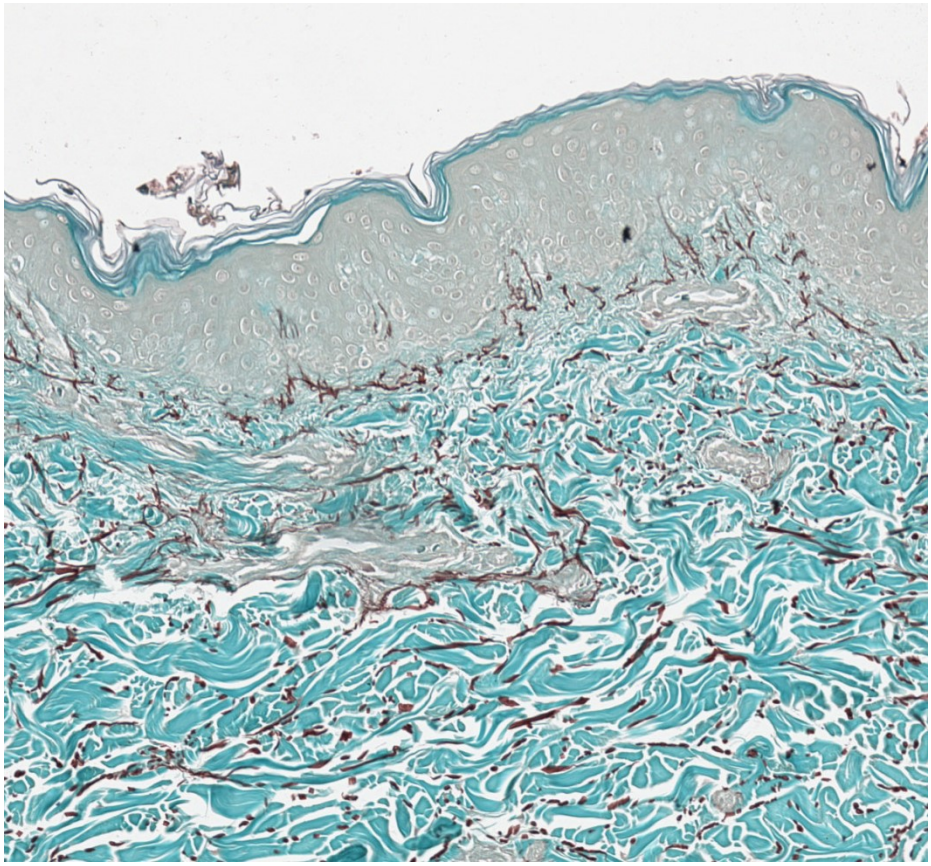

Figure 2: Human skin sample stained with Orcein Elastin Stain and Light Green
OES: dark brown fibres; Light Green: blue-greenish counterstain (×240)

Right after these steps Light Green was applied as a counterstain. The ingredients for this solution are 0.2mg of Light Green SF yellowish, 100ml of distilled water and 0.2ml of glacial (anhydrous) acetic acid. 10ml of this Light Green solution diluted by 50ml of distilled water were applied to the slides right after being washed in tap water (38):

- Light Green in distilled water; 1:6 (45s) (38)
- 95% ethanol (2min)
- Absolute ethanol (4 pots, up to 2min each)
- Xylene (2 pots, 1min each)

2.3 Coverslipping

After the stainings were done the undried slides became coverslipped: A drop of xylene-based mounting agent was placed onto the tissue and a glass cover was attached. Right before coverslipping the tissue did not become dried in order to leave enough liquidity in and around the tissue to avoid the occurrence of air bubbles between the tissue and the coverslip. (33)

The process of coverslipping was carried out by the Leica CV5030 Coverslipper which is connected in series with the Leica ST5010 Autostainer XL, as mentioned in *Section 2.2.1*. Hereby, sections stained with H&E using the autostainer were simply passed onto the coverslipper which applied a xylene-based mounting medium. (37)

2.4 Picturing

In order to analyse the stained slides, they first needed to be scanned to create a digital image of them. These images were required to depict enough detail to let a computer program extract the data needed for image processing.

2.4.1 Bright-field microscopic picturing

Physical bases and components of bright-field microscopes

The mechanisms of a bright-field microscope, its main components and the way the light passes through them is shortly described in this section. The following descriptions relate to a conventional upright microscope:

The light is emitted by a light source and gets focused by a collector lens. The light – now following a horizontal way – passes through a couple of filters (e.g. a daylight filter) which can be removed or added for certain requirements. The light subsequently reaches a mirror which now leads it vertically through an aperture called the field diaphragm which determines the exact area of the slide to get illuminated. This aperture plays a crucial role in setting the Köhler illumination correctly. The Köhler illumination guarantees a homogeneous illumination of the slide area which is currently under observation without compromising the resolution of the image produced. (41)

The next component which the light rays reach is the condenser. It consists of an aperture stop which determines the angle of the light cone illuminating the tissue area under investigation by narrowing or widening its opening. The condenser is vertically adjustable and firmly connected to the stage which provides the spot where the tissue slides are placed. Hence, the condenser determines the distance between the specimen and the following objective lens and therefore is used for focusing. (41)

The following part of the microscope is called the nose piece and consists of a series of replaceable objective lenses with different magnifications which allow the observer to change the magnification while observing a slide. The next and last piece of a microscope

is called the body tube which contains the eyepiece (ocular lenses) and directs the light rays to the observer's eye. (41)

The magnification of a microscope depends on the magnification factors of two microscope components: the objective lenses and the ocular lenses. The product of the multiplication of these two factors gives the overall magnification. For the actual interpretation of a slide, however, the resolution is another crucial factor to be considered. The term resolution is defined by the smallest distance between two visual points which can still be perceived as such and can be described by the numerical aperture (NA) of an objective. The NA describes the amount of light passing through a specimen (including effects like diffraction) an objective can gather and corresponds to the resolution. Hence, a high NA indicates a high resolution (41):

$$NA = n \times (\sin \mu)$$

The formula above describes how to calculate the NA, n representing the refractive index which depends on the transmission medium between specimen and objective (defined as 1 for air) and μ representing half the aperture angle of the trespassing light. Consequently, the resolution increases with a transmission medium of a higher refractive index and with a higher aperture angle, meaning a shorter distance between specimen and objective. (41)

If white light passes through a conventional lens it becomes split up into its colour fractions. To correct this unpleasant side effect most digital microscopes nowadays consist of apochromatic lenses which provide identical focuses for every colour within the visible spectrum of light and even beyond. (41)

The above described microscope components can be found in an upright microscope. Especially digital microscopes are usually constructed differently, and then referred to as inverted microscopes. Also, the eyepiece is a component which often does not exist in microscopes used to produce digital images of specimens. Since I only intended to describe the principle mechanisms of microscopes which are the same in every bright-field microscope I am not going into detail about the differences between manual upright microscopes and digital ones. (41)

Picturing process

I scanned both the H&E-stained slides, as well as the slides stained with OES with a bright-field microscopic scanner. The scans of the slides stained with OES were necessary to quantify the amount of elastic fibres using a computer program while the H&E-stained

slides were scanned mainly to compare the appearance of solar elastosis in both stains with one another.

For the scanning process I used an Aperio® ScanScope XT. I scanned the slides stained with OES using an objective of a 20× magnification while the H&E slides' scan were obtained with an objective of a 40× magnification. For the assessment, the digital analysis and the comparison between these different stains I only required the 20× objective. However, I scanned the H&E stained slides using an objective of a magnification of 40× because these scans were also needed for investigations in a different project. The two objectives of 20× and 40× magnification correspond to resolutions of 0.5µm and 0.25µm per pixel, respectively. (42)

2.4.2 Fluorescence microscopic picturing

Physical principles of fluorescence and construction of a fluorescence microscope

If an electron absorbs a photon which has an energy level of exactly the difference between the energy level of the mentioned electron and the next energy level the electron can reach, it can be elevated to exactly that next energy level. In this higher, yet instable energy level the electron loses some of the recently gained energy before it emits the rest of it in the shape of a photon and falls back into its basal stable energy level. The sum of all these photons emitted from a bulk of electrons with the above described characteristics appears to us as fluorescence. As a consequence of how fluorescence light emerges, the wavelength of the exciting light is always shorter than the wavelength of the emitted (fluorescing) light. The difference between these two wavelengths/energetic levels is referred to as Stokes shift. A chemical substance with the ability to fluoresce is termed a fluorochrome or a fluorophore. (41)

While the light source in a bright-field microscope is situated behind the specimen and the image results from the subtraction of light rays which become absorbed or diffracted by the specimen, the light sources in a fluorescence microscope is the flourochrome situated in the specimen itself. Hence, the fluorescence image of the specimen is being created by the sum of emitted rays which originate from the specimen under investigation. Of course, the fluorochromes which are situated in the specimen need to be excited by another light source. The pathways of both the exciting light and the emitted light, along with the construction of a fluorescence microscope shall be described in the following (41):

The energy source which sends off the flourochrome exciting rays is usually a high-pressure metal vapour lamp using metals like mercury or xenon. The exciting light rays become bundled by a couple of lenses which direct them towards a bandpass (BP) filter, called an excitation filter. This filter either absorbs (absorption filter) or reflects (interference filter) the light rays of wavelengths beyond the spectrum needed to excite the fluorochrome. (41)

Those rays which pass the excitation filter now reach a mirror which stands in a 45° angle to the direction the light comes from. Because of its special characteristics this mirror is called a dichromatic mirror (see below) and it directs the exciting light rays towards the objective lenses. In this context the objective lenses focus and direct the exciting light rays exactly into the currently observed specimen region. Consequently the rays excite the flourochromes of the specimen which then emit fluorescence light. Some rays of this light reach the objective which now fulfils the same purpose as it does in a bright-field microscope (see *Section 2.4.1*). (41)

The gathered fluorescence light rays reach the dichromatic mirror which directed the excitation light towards the specimen. But instead of being redirected the fluorescence light passes right through the mirror. A dichromatic mirror is characterised by the ability to reflect wavelengths below a certain threshold and to let higher ones pass right through it. Because of the Stokes shift (see above) both wavelengths of the excitation and the fluorescence light are known. The dichromatic mirror's threshold wavelength is chosen in a way that only the excitation light but not the fluorescence light becomes reflected. (41)

The next microscope component the fluorescence light needs to pass is the suppression filter which allows only a very narrow spectrum of wavelengths to reach the microscope's eyepiece. This filter can either be a BP or a long-pass filter which separates the specific fluorescence light from any reflections or other beams that might occur. (41)

The objective lenses in fluorescence microscopes are mostly apochromatic to guarantee a very high NA but at the same time deliver chromatic correction. The chromatic correction becomes even more important the higher the Stokes shift between excitation and fluorescence light is. (41)

Picturing process

To capture fluorescence microscopic images I used the Aperio® ScanScope FL which offers a wide range of filter and dichromatic mirror sets. I scanned the slides using an

objective with a 20× magnification which corresponds to a resolution of 0.468µm/pixel. (43)

As mentioned in *Section 1.2.2.2*, in their article *Characterizing cutaneous elastic fibers by eosin fluorescence detected by fluorescence microscopy* YS Heo et al describe the loss of autofluorescening activity of elastic fibres in photoaged skin. (7) *Table 2* depicts a comparison between the filter and dichromatic mirror set used in the original article by YS Heo et al (7) (column *FITC)* and the filter and dichromatic mirror set used in this thesis (column *Alexa 488*).

Original dye created for	FITC	Alexa 488
Excitation filter	BP 465/30nm	BP 490/50nm
Dichromatic mirror: threshold	505nm	505nm
Suppression filter	515nm barrier filter	BP 527/30nm

Table 2: Comparison of filters and mirrors used in Y. Soo Heo et al (7) (FITC) and here (Alexa 488)

As listed in *Table 2* the filter and dichromatic mirror set used by YS Heo et al (7) slightly differs from the one I used. However, the same fluorescent fibres as depicted in YS Heo et al's Fig. 1B (7) could be seen in skin samples of little sun exposure using the filter and dichromatic mirror set I did (see *Figure 3*, left image). These fibres could not be found in

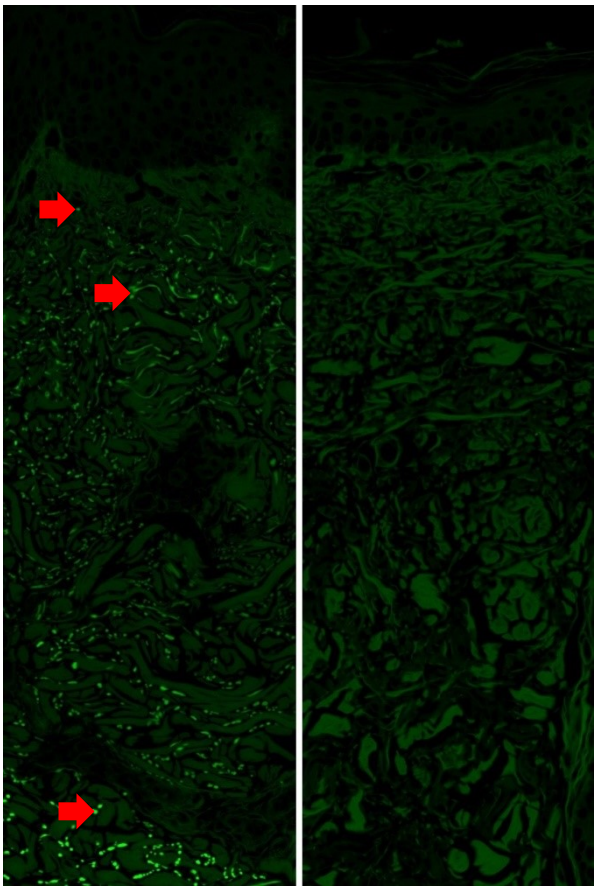

Figure 3: Comparison of autofluorescence patterns between mild (left) and marked (right) photoaging
Left specimen was obtained from the neck of a 24-year old female, assigned to "mild" solar elastosis, *red arrows* point at autofluorescent elastic fibres; right specimen was obtained from the back of a 79-year old male, assigned to "marked" solar elastosis, more than 0.5mm in the depth no autofluorescent elastic fibres can be found in.
Both samples: H&E, fluorescence microscope, ×200.

sun-exposed skin samples (see *Figure 3*, right image), corresponding to YS Heo et al's Fig. 4B (7). Hence, despite slight differences in the filter and dichromatic mirror sets applied, the same results regarding H&E stained elastic fibres could be obtained.

The filter and dichromatic mirror set I used was originally created for a fluorochrome called Alexa Fluor® 488. This fluorochrome can be applied to histological sections in order to highlight specific tissue components in fluorescence microscopy. Of course, I did not add any fluorochrome to the specimens but captured the autofluorescent activity of H&E stained elastic fibres which happen to absorb and emit similar wavelengths as the Alexa Fluor® 488 dye. Hence, I could use the filter and dichromatic mirror set originally created for this fluorochrome. (44,45)

Table 2 contains a series of descriptions about the two filter and dichromatic mirror sets compared which shall briefly be explained: Both of the excitation filters and the suppression filter of the Alexa 488 set are band-pass filters (BP) which are defined by the mean wavelength X (in nm) and the width Y (in nm) of the wavelength spectrum in which the transmission rate of electromagnetic waves is at least 50% (BP X/Y). The suppression filter of the FITC set is a long-pass filter which allows any wavelength longer than its threshold (in nm) to trespass but blocks any wavelength below. The dichromatic mirror is defined by the wavelength (in nm) which creates the low threshold for electromagnetic waves to trespass. In other words, any wavelength longer than this threshold can pass through while any wavelength shorter becomes reflected. Hence, the mirror reflects the rays of the exciting light but lets the emitted fluorescence rays trespass. (41)

Another parameter which needed to be adjusted was the exposure time which determined how long the objective would focus on one single spot of tissue. (43) Since the image produced represents the sum of all fluorescence rays captured by the detector of the microscope within this predefined time the brightness of the fluorescence image correlates to this parameter.

I applied the exposure time of 0.2ms to every slide. The images I obtained from this adjustment allowed me to clearly identify and distinguish the different skin layers due to gentle background fluorescence of non-elastic tissue components and hence enabled me to orientate myself within the slide. At the same time these images did not depict non-elastic fibre tissue as bright as healthy elastic fibres. In other word, both the identification of healthy elastic fibres and the measurement of their depth were possible.

A few slides, however, presented with highly elevated fluorescing activity of large areas of dermal tissue which did not allow differentiation between healthy elastic fibres and non-elastic fibre tissue any more. In the following I will refer to these slides as “overexposed”.

When looking at overexposed slides under a manual bright-field microscope they appeared to carry thicker tissue ribbons than non-overexposed ones since I could focus on more layers of keratinocytes within the epidermis. So my explanation for the increased dermal tissue brightness in overexposed slides was their increased tissue thickness and the concomitant increased background fluorescence of non-elastic fibre tissue. The inequality in thickness between tissue ribbons seemed to have emerged from the process of sectioning since the tissue appears smooth and free of folds.

One approach to face this problem was to decrease the exposure time in every slide. At this point it is important to note that the microscopic scanner (Aperio® ScanScope FL) needs a certain level of background fluorescence of the tissue to focus on in order to take an image. Since the images of most slides depicted a rather faintly fluorescing dermis and therefore drastically reduced exposure times would not allow the microscope to focus on any tissue any more I discarded this approach.

Most of the overexposed images, however, also contained areas with a lower level of background fluorescence (mostly close to the margins of the tissue samples) which did allow differentiating between elastic fibres and non-elastic fibre tissue. The fluorescence level of these areas was comparable to the background fluorescence in non-overexposed slides. By using these marginal areas for my measurements I only had to exclude one slide from the analysis due to too large overexposure regions.

2.5 Evaluation

The next step was to extract the data from the histological scans which consequently could be used to investigate if there was a correlation between the quantification of OES stained tissue (PM), the loss of fluorescence activity in elastic fibres (LoFM) and the assessment of the degree of solar elastosis by pathologist.

2.5.1 The Positivity-Method

Solar elastosis is defined as the accumulation of elastotic fibres or elastotic bulk in deeper layers of the papillary dermis and the reticular dermis. Hence, to equally assess the relative amount of elastic/elastotic fibres I decided to quantify the OES in each slide in an area

ranging from the basal papillary dermis 500µm into the depth. I oriented myself towards the basis of the dermal papillae and looked for the level at which superficial elastic fibres could be found. At this level I drew a horizontal line, applied another length of 500µm into the depth and drew a parallelogram: The base of this parallelogram was the horizontal line and its height was applied 500µm into the depth of the skin sample. I decided to draw parallelograms rather than rectangles in order to reconstruct the skin's physiological orientation which sometimes appeared distorted due to pre-staining preparations. These distortions can develop since the skin samples are not under physiological tension as they are when integrated in the human body.

Since solar elastosis is described as a band-shaped mass evenly spread parallel to the skin surface the length of the parallelogram's basis would not have an impact on the results. Hence, I adjusted its length to the individual characteristics of the slides: I tried to set it rather large but at the same time avoided to imply any skin appendages like glands or hair follicles into the area of analysis because these structures would appear as elastin-free and would therefore wrongly decrease the quantification's results. Depending on the amount of skin appendages and the infiltration of the tumour (which I avoided to integrate into my analysis) the length of the parallelograms' bases ranged between 200µm and 600µm.

Due to the wavy course of the dermo-epidermal junction I sometimes had to adjust the parallelogram's baseline to the individual surface bending of the slides (see *Figure 4*).

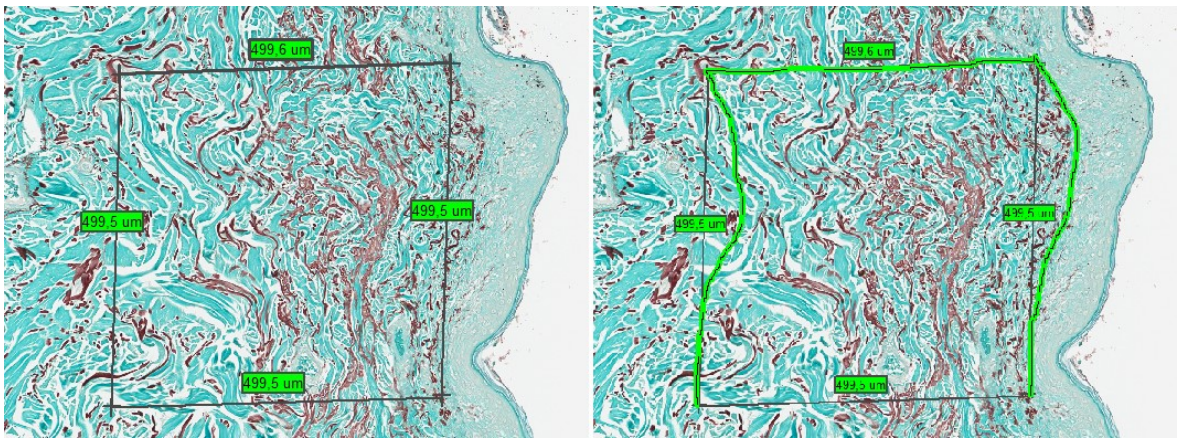

Figure 4: Taking measurements (left) and defining a region (right, *green shape*) for subsequent analysis
Note that the parallelogram's shape has been adjusted to the surface bending of the slide. The depth of the ribbon-shaped region, however, is evenly 500µm. (×90)

2.5.1.1 **Analysis program**

I accessed the digital scans of the specimens via ImageScope (by Leica Biosystems) which is a viewing software specifically created for this usage.

One analysis feature of ImageScope is called Positive Pixel Count (PPC). It allows the user to scour a previously defined specimen region for pixels of a hue tone they are interested in. There are a couple of parameters that need to be adjusted in order to establish an analysis algorithm which can then be applied to regions of specimens. In the following I am going to briefly describe the most important ones of these parameters to understand the concept of PPC (46):

- ***Hue value***: The colour spectrum detected by a human eye is virtually spread continuously over a circle. At the same time values between 0 and 1 are assigned to each point of the circle and thus to every colour: The values 0 and 1 are both defined as a pure red and hence are equal in this scheme, 0.33 is defined as pure green, 0.66 is defined as pure blue (this value-colour attribution is depicted in a linear way in *Figure 5*, see below). Since the spectrum is continuous numbers between 0 and 0.33 are attributed to colours between red and green; the closer it gets to 0.33, the more the colour turns into a green hue. As a result of the described, brown is defined as 0.1. The parameter "hue value" is defined as the number (between 0 and 1) attributed to the hue of interest for the analysis. (46)

Figure 5: Depiction of hue values assigned to colours in accordance with the system of a colour circle

- The ***hue width*** (x) defines the width of the range around the hue value (y) representing colours which shall be recognised as positive. Hence, every pixel with a colour value within the range $y - \frac{x}{2}$ to $y + \frac{x}{2}$ will be recognised as positive. For example, if the hue value was set at 0.3 and the hue width was set at 0.1, every pixel within an annotated specimen region of interest would be recognised as positive if its hue value was between 0.25 and 0.35. (46)
- Every pixel of a digital slide can be divided into a colour component and a grey component. The sum of these two is always 1, hence, the stronger the colour component, the weaker the grey component. The ***colour saturation*** is defined as the colour component of this ratio and ranges between 0 being a grey pixel without any colour and 1 being a pixel without any grey component. In other words, the hi

- gher the colour saturation is set the purer the colour has to be in order to be interpreted as a positive pixel by the program. (46)
- The ***intensity*** of a pixel refers to its brightness. In this program there are 256 ($= 2^8$) discrete steps of brightness ranging from 0 being black to 255 being white. A "high intensity threshold" defines how bright a positive pixel is allowed to be and is applied in order to prevent very faint stains (mostly unspecific bindings; also called "background stain") from being recognised as positive; the "low intensity threshold" is usually set at 0 (black). Intensity is also used to differentiate levels of positivity. These levels are termed – assorted from high intensity to low – weak positive (wp), medium positive (p) and strong positive (sp). The higher the intensity of a pixel is, the weaker the positivity is interpreted by the program which can be explained by the way a bright-field microscope works (see *Section 2.4.1 - Physical bases and components of bright-field microscopes*): Since a stain partially absorbs the light which trespasses the slide, the brightness of a specimen region declines with the affinity of the stain to this region. (46)

One value the PPC feature calculates is the positivity of the selected slide area. The positivity P of an area is defined as the quotient of the number of positive pixels (wp+p+sp) p divided by the total number of pixels evaluated (positive and negative) t ($P = \frac{p}{t}$). It is important to note that every pixel in the area of analysis with a higher intensity than the high intensity threshold – irrespectively of their hue – does not become integrated in the evaluation. I still decided to use the positivity for my results since pixels with very high intensity could mainly be found at minor gaps within the slides representing extracellular fluids and fat. Hence, I quantified the tissue stained with the OES and put it in relation to the entire tissue in the area of analysis without including fluids and fat. (46)

As mentioned in *Section 2.2.2*, the OES does not allow differentiating between healthy elastic fibres and elastotic tissue. Hence, the obtained results can never be 0, even in samples without any elastotic changes.

2.5.1.2 **Analysis algorithms**

Since the hue of the OES is brownish, the hue value of an analysis algorithm designed to find pixels stained with it had to be set somewhere around 0.1. Since the counterstain Light Green is described as a green tone and on the scans obtained it appeared like a green-bluish

hue, the hue value of the counterstain was probably somewhere between 0.33 and 0.66. Hence, I did not have to set the hue width very narrowly.

Soon, it was apparent that a hue value of 0.05 and a hue width of 0.2 covered the OES very well and still did not recognise the counterstain as positive at all.

After every run of analysis a window on the computer screen visually depicts the analysis of the selected region: Negative pixels are displayed in a dark blue colour, weak positive pixels in yellow, medium positive pixels in orange and strong positive ones in red. Pixels with intensities beyond the high intensity threshold are depicted as white pixels. Since weak positive pixels are presented in a yellow hue which can sometimes be quite difficult to distinguish from white pixels, I changed the intensity threshold values so that weak positive pixels were displayed as medium positive ones (in an orange colour). In other words, the visual analysis only differentiated between medium and strong positive pixels. The high intensity threshold of the analysis, however, stayed the same. Since the analysis output positivity P does not differentiate between the different levels of positivity ($P = \frac{wp+p+sp}{t}$) the above described changes to the intensity thresholds did not have any effect on the numerical analysis results.

In some samples the counterstain Light Green appeared to be much stronger (darker) than in others, the reason of which I could not entirely clarify. However, when looking at the nuclei within the epidermis under a manual bright-field microscope in specimens with a stronger counterstain I could focus on more layers of nuclei than in the ones with a fainter counterstain. The same phenomenon was observed when looking at overexposed slides in the LoFM (see *Section 2.4.2 – Picturing process*). Similar to the interpretations of overexposed slides in the LoFM, the explanation of increased tissue thickness seemed satisfactory here too: Thicker tissue ribbons can trap more of the counterstain's dye and under a bright-field microscope appear more strongly stained. Another reason for an unequally strong counterstain could be that some runs of slides remained longer in the counterstain pot. Since the slides stained with OES and Light Green passed the pots accordingly to a strict time schedule the staining process itself was unlikely to have caused this effect.

Irrespectively of the causes of the counterstain's different appearance I decided to establish two different algorithms: One for the slides with a light counterstain and one for those with a heavy one:

- I named the algorithm established for slides with weaker counterstains ***OES2***: I applied a colour saturation threshold of 0.1 (meaning saturations between 0.1 and 1 are recognised as positive) which made this algorithm quite sensitive. Since stain and counterstain obviously had very different hue values I only required little purity of the target hue. The high intensity threshold for medium positive pixels was set at 235 and the threshold between medium and strong positive was set at 176. Stains with weak counterstains sometimes presented areas with faint OES background, representing unspecific OES stains (see *Figure 6*), which is why the high intensity threshold was set slightly lower than in OES3 (see below).
- ***OES3***: The algorithm which I applied to slides with stronger counterstains had an even lower colour saturation threshold of 0.01. This algorithm accepts a stronger grey component to the hue; it recognises colours even less pure than algorithm OES2. An increased grey component was required to be accepted because of the increased thickness of the tissue ribbon in these slides leading to increased absorption of trespassing light and decreased intensity and colour saturation. Furthermore, in thicker tissue ribbons it was more likely that single beam paths could pass through both OES stained fibres and other dermal components which would further decrease the purity of the hue. Since – as discussed above – this algorithm was intended to be more sensitive than OES2 the high intensity threshold for medium positive pixels was set at 240. The intensity threshold between medium and strong positive pixels was set at 176, as it was in OES2.

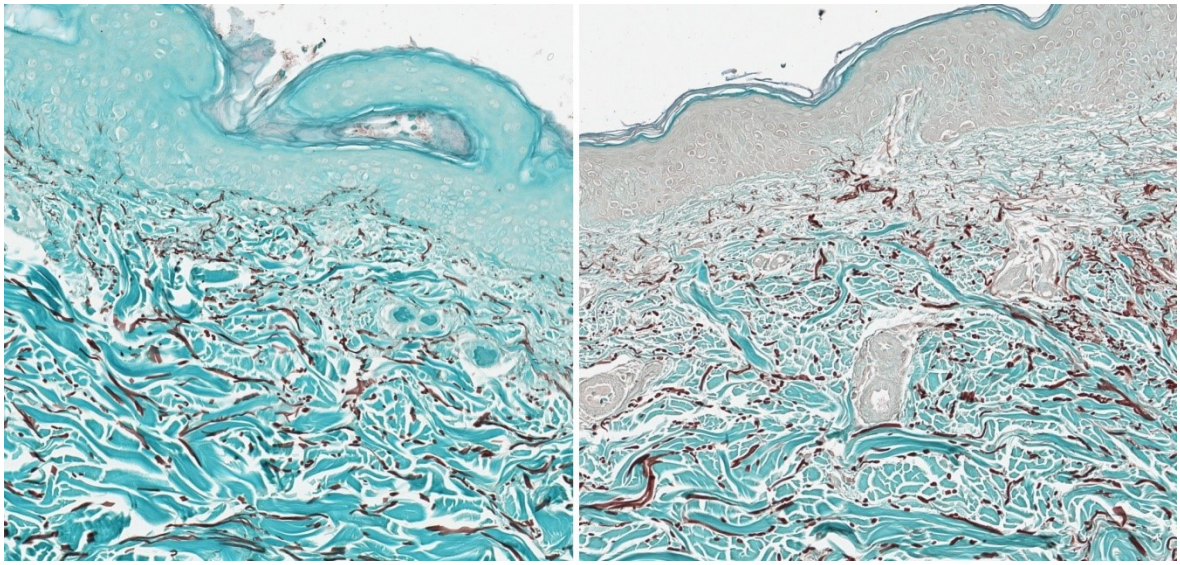

Figure 6: Comparison of slides analysed with OES3 (left) and OES2 (right)
Note hue differences at the epidermis and blood vessels: faint red hue as unspecific dye of OES (right) vs. blue-greenish hue as counterstain of Light Green (left); magnification in both slides: ×145

(OES1 was the first algorithm established. It did not recognise the target hue as specifically as the other two algorithms and therefore did not get applied to any slides for analysis)

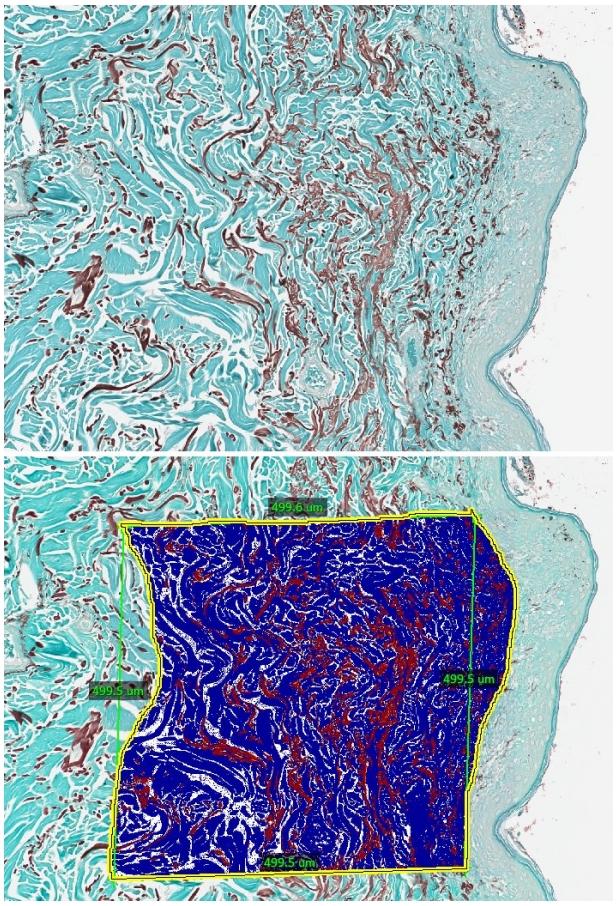

Figure 7: Algorithm OES3 applied to OES stained slide of moderate solar elastosis
Skin sample obtained from the back of a 77 year old male patient (×100); lower image depicts the visualised assessment of the sample's pixels within the predefined area of interest: *Blue pixels*: negative, *Orange pixels*: medium positive, *Red pixels*: strong positive

2.5.2 The Loss of Fluorescence-Method

The degree of accumulated solar irradiation on human skin correlates to the depth of the most superficial elastic fibres which still have the ability to fluoresce stronger than their immediate surrounding (see *Section 1.4*). In each digital slide I marked the level from which on the elastic fibres' autofluorescence allowed differentiating them from other kinds of dermal fibres at three different spots. I then measured the shortest distances from these three marked points to the apical ends of the dermal papillae (see *Figure 8* below). Intending to minimise the impact of possible outliers I decided to use the median of these three values for the consequent statistical analysis.

In some slides I observed clusters of brightly autofluorescent thin fibres. These clusters were about 100µm in diameter and were frequently situated closer to the surface than the overall level of the most superficial autofluorescent elastic fibre. I decided not to use these

clusters for the measurements of the loss of autofluorescent activity in elastic fibres and therefore not to include them in my analysis. I rather pictured these clusters to be newly synthesised, healthy elastic fibres which had not been exposed to solar irradiation long enough to lose their autofluorescent activity. Of course this is just my conjecture but it seemed obvious that these random clusters of brightly fluorescing fibres did not represent the overall level to which solar irradiation impaired the H&E-stained elastic fibres' ability of autofluorescence.

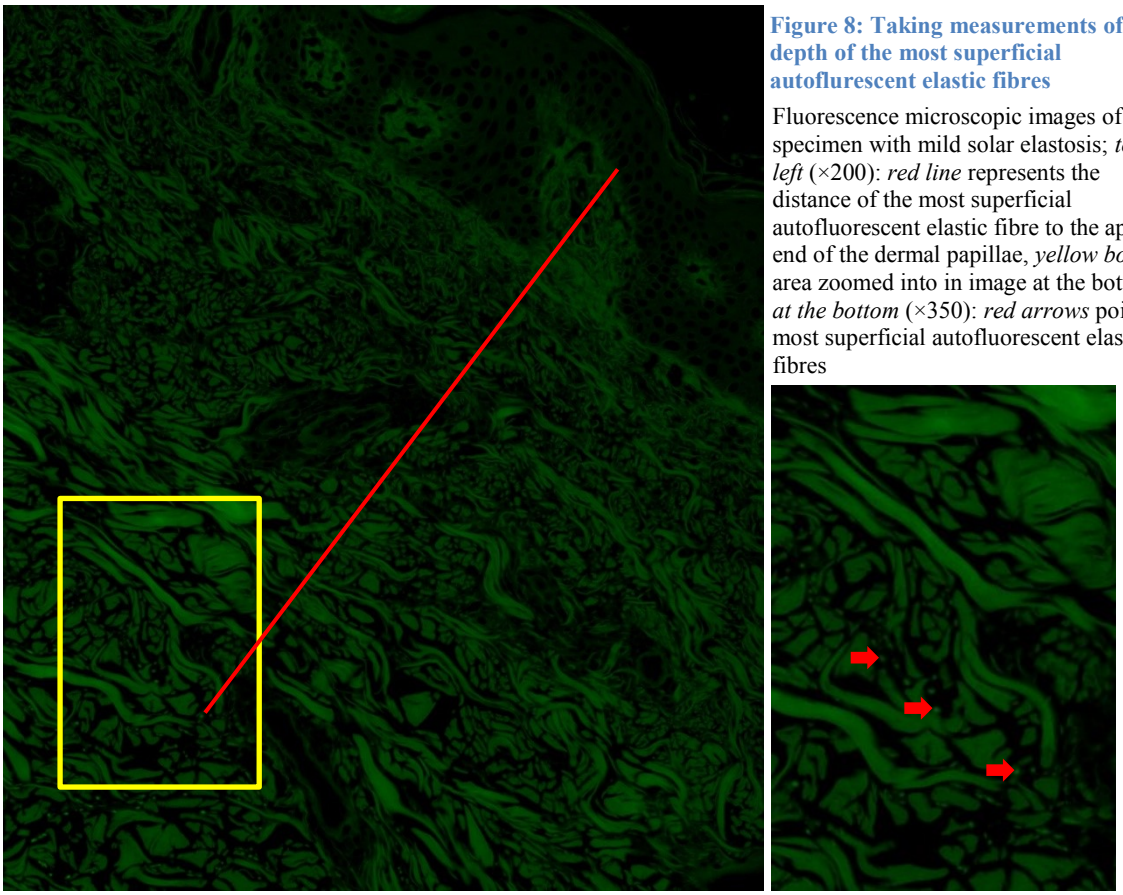

Figure 8: Taking measurements of the depth of the most superficial autoflurescent elastic fibres

Fluorescence microscopic images of a specimen with mild solar elastosis; *to the left* (×200): *red line* represents the distance of the most superficial autofluorescent elastic fibre to the apical end of the dermal papillae, *yellow box*: area zoomed into in image at the bottom; *at the bottom* (×350): *red arrows* point at most superficial autofluorescent elastic fibres

2.6 Statistical testing approaches

2.6.1 Graphical overview

In order to illustrate the distribution of the obtained values and to visually compare both quantification methods I inserted the results into a MS Excel file. I intended to depict every relevant feature in one chart so that one figure would visualise the data obtained from both the PM and the LoFM as well as the pathologists' semiquantitative evaluation.

I created a scatter plot, in which I applied the values from the PM as the x-coordinate and those from the LoFM as the y-coordinate. I also included the pathologists' evaluations of the specimens' degree of solar elastosis by assigning different symbols or different colours to the specimen representing values.

2.6.2 Inferential statistics

In order to mathematically test the results of my methods I entered the data obtained from the PM, the LoFM as well as the pathologists' evaluation into an IBM SPSS Statistics file (Version 22).

2.6.2.1 **Creating and testing possible value limits**

First of all I decided to calculate value limits for both the positivity of the PM and depth of autofluorescent elastic fibres of the LoFM between the different semiquantitative categories of solar elastosis used by the Australian pathologists. I chose those values as value limits which offered the highest Youden's index (= sensitivity + specificity – 1), in other words, I ascribed the same importance to the sensitivity and the specificity. By creating these value limits and calculating their accuracy (sensitivity and specificity), I was seeking to determine if the obtained values correlated with the pathologists' evaluations. (47)

Since the amount of solar elastosis in only three slides was classified as "nil" by the pathologists and I required classes consisting of larger specimen groups I decided combine the two classes of "nil" and "mild" solar elastosis, creating a new group "nil-mild". In the following I only calculated the value limits between three instead of four classes.

Another four specimens have not been evaluated by pathologists, thus, I had to exclude those from this statistical analysis step.

In order to calculate value limits I created separate ROC (receiver-operator characteristic)-curves for the PM values and the LoFM values. In a first run I applied the number 0 to every specimen classified as "nil-mild" and 1 to every specimen classified as "moderate" or "marked". In a second run I applied the number 0 to every specimen classified as "nil-mild" or "moderate" and 1 to every specimen classified as "marked". Thereby I (twice) created two value groups I was interested in calculating value limits for, which would separate these two groups as accurate as possible.

Generally, the ROC-analysis tests a series of values for their accuracy in respect of their ability to separate two predefined groups. (47) More specifically, it calculates the arithmetic mean between every two subsequent numbers of a list of values sorted by size and tests every one of these means for its specificity and sensitivity as a value limit.

After the ROC-analysis had calculated the specificity and sensitivity for the list of possible value limits I entered the results into an MS Excel table, calculated the Youden's index (see above) for each of the tested values and looked for the highest outputs in each run. (47) This way I received those value limits with the highest sum of specificity and sensitivity for both quantitative methods between nil-mild and moderate as well as moderate and marked elastosis levels.

2.6.2.2 **Correlation between the two methods**

I also wanted to calculate the correlation coefficient between the two methods established in this thesis. Unlike in the previous statistical test, for this mathematical analysis I did not need to exclude the four specimens which were not classified by pathologists.

I calculated both the Pearson product-moment correlation coefficient the Spearman's rank correlation coefficient to mathematically express the degree of linear and monotone correlation, respectively. (48) The significance level for both correlation coefficients was set at 0.01 (for two-tailed testing).

Expecting a stronger linear correlation I calculated the decade logarithm of the positivity values obtained from the PM and determined the degree of linear correlation between these transformed values and the values obtained from the LoFM by calculating the Pearson product-moment correlation coefficient again.

3 Results

Initially 55 specimens were included for testing the two methods described in detail in *Chapter 2*. Since the histological condition of six specimens did not meet the laboratory criteria only 49 could be included in my analysis. Reasons for exclusion are listed in the following:

- Two of the specimens were obtained too superficially to either quantify the amount of tissue that had the staining characteristics of elastic fibres within a 500µm band beneath the epidermis (OES) or to find autofluorescent fibres in H&E stained slides and then measure their distance to the surface.
- One H&E stained specimen depicted large areas of strongly fluorescing fibres, presumably due to a too large thickness of the tissue ribbon (see *Section 2.4.2*), which did not allow the differentiation between elastic and non-elastic fibres. Hence, measurements could not be taken.
- Three specimens included large amounts of infiltrative melanoma cells which distorted the entire specimen and did not allow any measurements.

As previously reported (see *Sections 1.2.2.2* and *2.6.2.1*), four of the 49 specimens were not assigned to one of the four categories by Australian dermatopathologist and thus could not be used to determine threshold values between these categories. However, these four slides were still used to test the correlation between the two methods established in this thesis.

For the computer-based quantification of elastin-positive tissue in OES stained slides I applied algorithm OES2 to 20 slides and algorithm OES3 to 29 slides.

3.1 Histological scans and statistical overview

Figure 9 on *page 46* illustrates a comparison of light microscopic pictures of the H&E and the OES slides as well as fluorescence microscopic pictures of the H&E slides of three specimens; one assigned to each solar elastosis categories “nil”, “moderate” and “marked” (Australian pathologists’ assessment). Visualised in these pictures, the portion of faintly basophilic and red-brown dyed fibres in H&E and OES stained slides respectively increases from “nil” via “moderate” through to “marked”, representing solar elastosis.

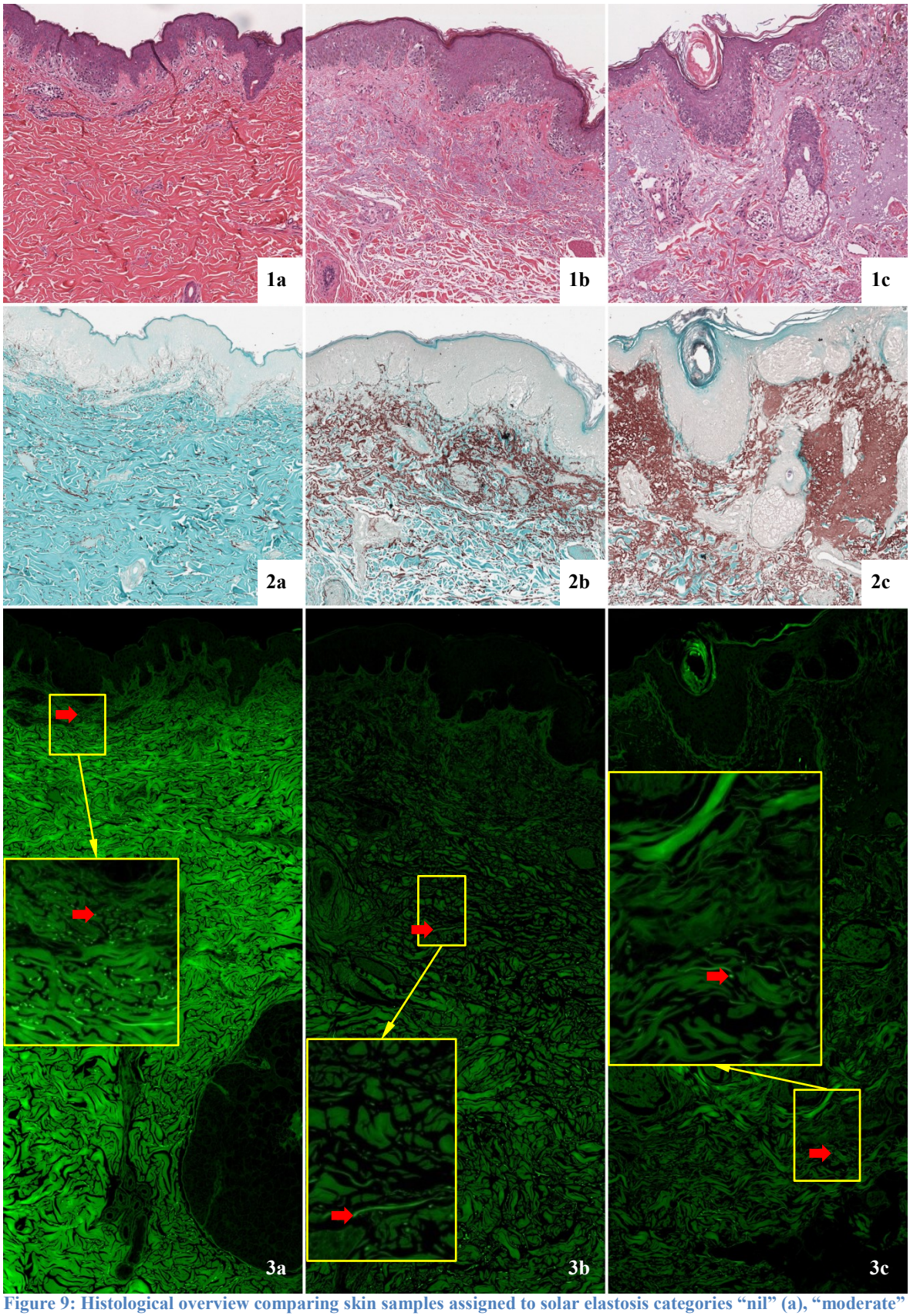

Figure 9: Histological overview comparing skin samples assigned to solar elastosis categories "nil" (a), "moderate" (b), and "marked" (c)

Row 1: light microscopic appearance of H&E stained slides (×51.3). *Row 2*: light microscopic appearance of OES stained slides (×51.3). *Row 3*: fluorescence microscopic appearance of H&E stained slides (×51.3); *red arrows* point at representative elastic fibres indicating the most superficial level at which autofluorescence allowed their identification; *large yellow boxes* depict areas at a higher magnification (×162.5) to show autofluorescent elastic fibres. Note vast differences between the intensity of background fluorescence (strong in *a*, weaker in *b* and *c*)

Accordingly, one has to go deeper into the tissue to find autofluorescent elastic fibres in samples with increased amounts of solar elastosis.

The results of all 49 specimens for both PM and LoFM, along with the assessment of Australian dermatopathologists are summarised in a diagram in *Figure 10* (see below).

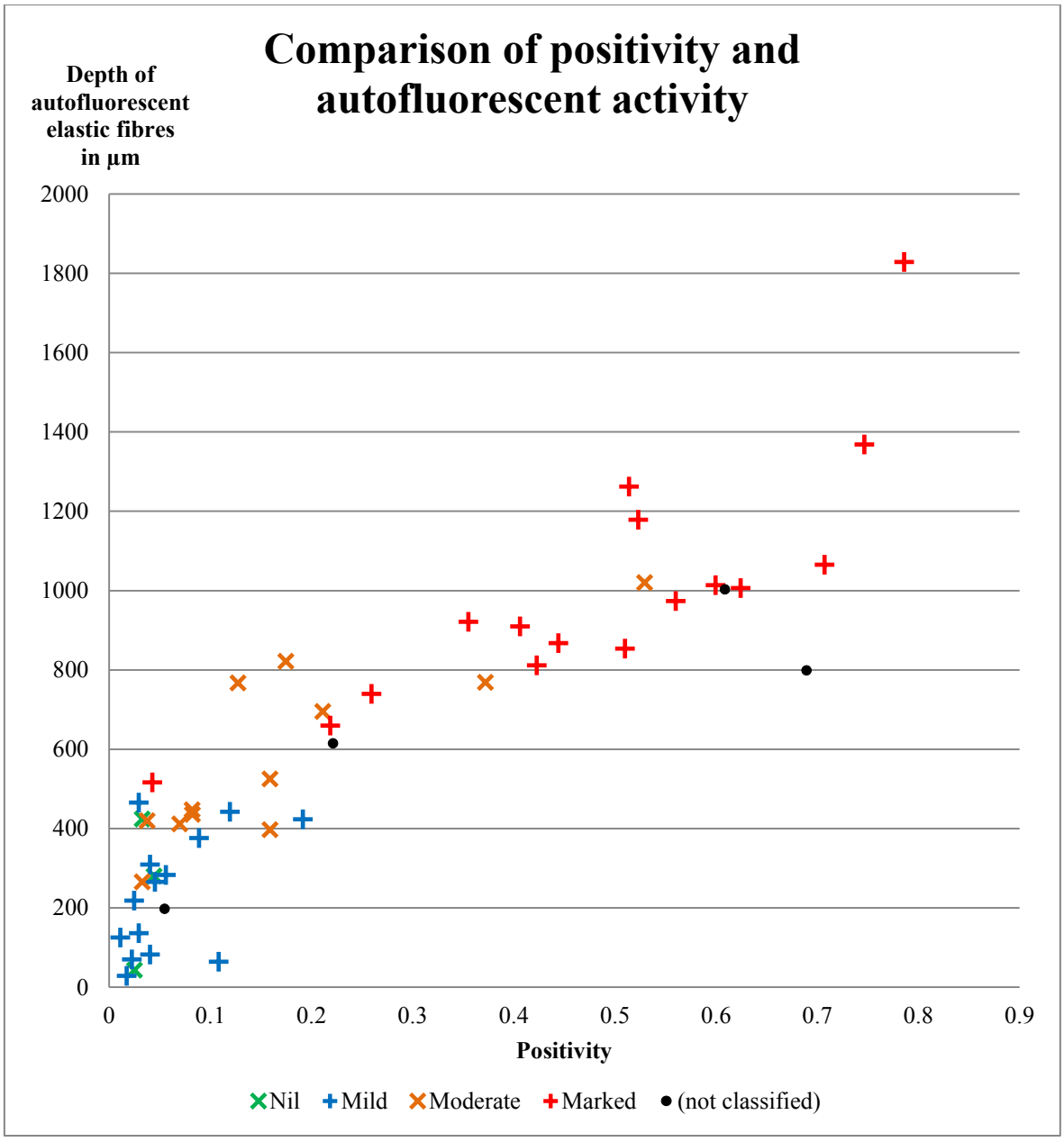

Figure 10: Statistical overview including the results of both methods and the histopathological evaluation of Australian dermatopathologists

When assessing *Figure 10* a few observations regarding the tested methods can be stated: First of all, three specimens are too few in order to represent a group, which is why the groups "nil" and "mild" have become combined to "nil-mild" (see also *Section 2.6.2.1*).

Within the method of determining the depth of the most superficial autofluorescent elastic fibres the highest value of group “nil-mild” is lower than the lowest value of slides assigned to group “marked”. “Moderate” specimens are distributed rather evenly between these two groups.

When assessing the distribution of the obtained values of OES stained slides (“positivity” in the PM) a quite similar impression emerges: Except for one sample of the group “marked” no overlap between “nil-mild” and “marked” can be observed. Again, values of “moderate” specimens are centred in between of the two other groups’ centres, maybe merging farther into the value range of “group “nil-mild” than into “marked”.

3.2 Threshold values between categories

Figure 11 (see below) depicts the ROC curves created to calculate those threshold values which provide the highest sensitivity and specificity.

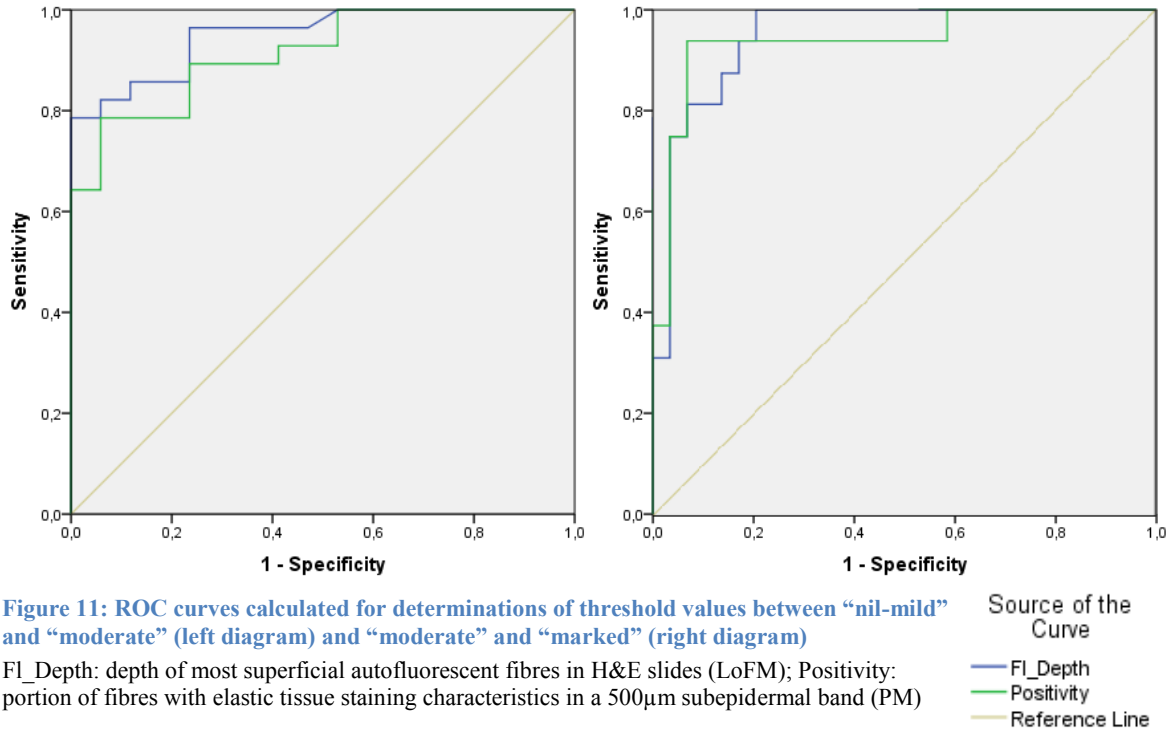

Figure 11: ROC curves calculated for determinations of threshold values between “nil-mild” and “moderate” (left diagram) and “moderate” and “marked” (right diagram)

Fl_Depth: depth of most superficial autofluorescent fibres in H&E slides (LoFM); Positivity: portion of fibres with elastic tissue staining characteristics in a 500µm subepidermal band (PM)

The Area under the Curve (AUC) values of the ROC curves for the threshold between “nil-mild” on the one hand and “moderate” and “marked” on the other hand for the LoFM and the PM are 0.951 and 0.914, respectively. The AUC values of the ROC curves for the threshold between “nil-mild” and “moderate” on the one hand and “marked” on the other hand are 0.948 (LoFM) and 0.938 (PM). AUC values close to 0.5 would indicate that there

is very little difference in the values between two groups. (49) The AUC values obtained here depict a good overall ability of the ROC to discriminate between two groups.

Table 3 (see below) quotes the value limits yielding the highest Youden's indexes calculated for both methods. By using the Youden's index (J) I have defined the value limits' sensitivity and specificity as equally important (J = sensitivity + specificity - 1).

Methods	Thresholds	Value	Sensitivity	Specificity	Youden's index
PM	**1***	0.123	0.786	0.941	0.727
	2**	0.215	0.938	0.931	0.869
LoFM (µm)	**1***	490.5	0.786	1.000	0.786
	2**	490.5	1.000	0.793	0.793

Table 3: Highest calculated Youden's indexes of possible threshold values in both methods
1*: threshold between „nil-mild" on the one hand and "moderate" and "marked" on the other hand;
2**: threshold between „nil-mild" and "moderate" on the one hand and "marked" on the other hand

Youden's indexes range between -1 and +1, whereat positive indexes are considered to indicate reasonable value limits. The higher the calculated Youden's index, the higher the sum of sensitivity and specificity, and hence the better the tested value limit's quality. (49)

As we can see in *Table 3* the Youden' indexes of the calculated value limits for both methods range between 0.727 and 0.869 and hence can be interpreted as reliable. One phenomenon which captures one's attention is the fact that both thresholds determined for the LoFM are the same value. This, of course, does not meet one's expectations regarding value limits between three semiquantitative categories and therefore will be discussed in *Section 4.2*.

The PM's thresholds between the three defined categories of solar elastosis "nil-mild", "moderate" and "marked" were calculated at 0.123 and 0.215. Together with the Youden's indexes depicted in *Table 3* these value limits indicate a high correlation between the dermatopathologists' evaluation and this method.

3.3 Correlation

The calculated correlation coefficients between the LoFM and the PM were 0.898 (Spearman's rank correlation coefficient) and 0.899 (Pearson product-moment correlation coefficient). The calculated two-tailed significances were 2.2×10^{-18} (Spearman) and 1.9×10^{-18} (Pearson) and hence way beyond the demanded significance level of 0.01.

The result of Pearson's correlation coefficient for the correlation between the values obtained from the LoFM and the logarithmic transformed values of the PM was calculated

at 0.879 (significance: 9.3×10^{-17}), presenting a slightly weaker linear correlation than when comparing the two non-transformed methods as such.

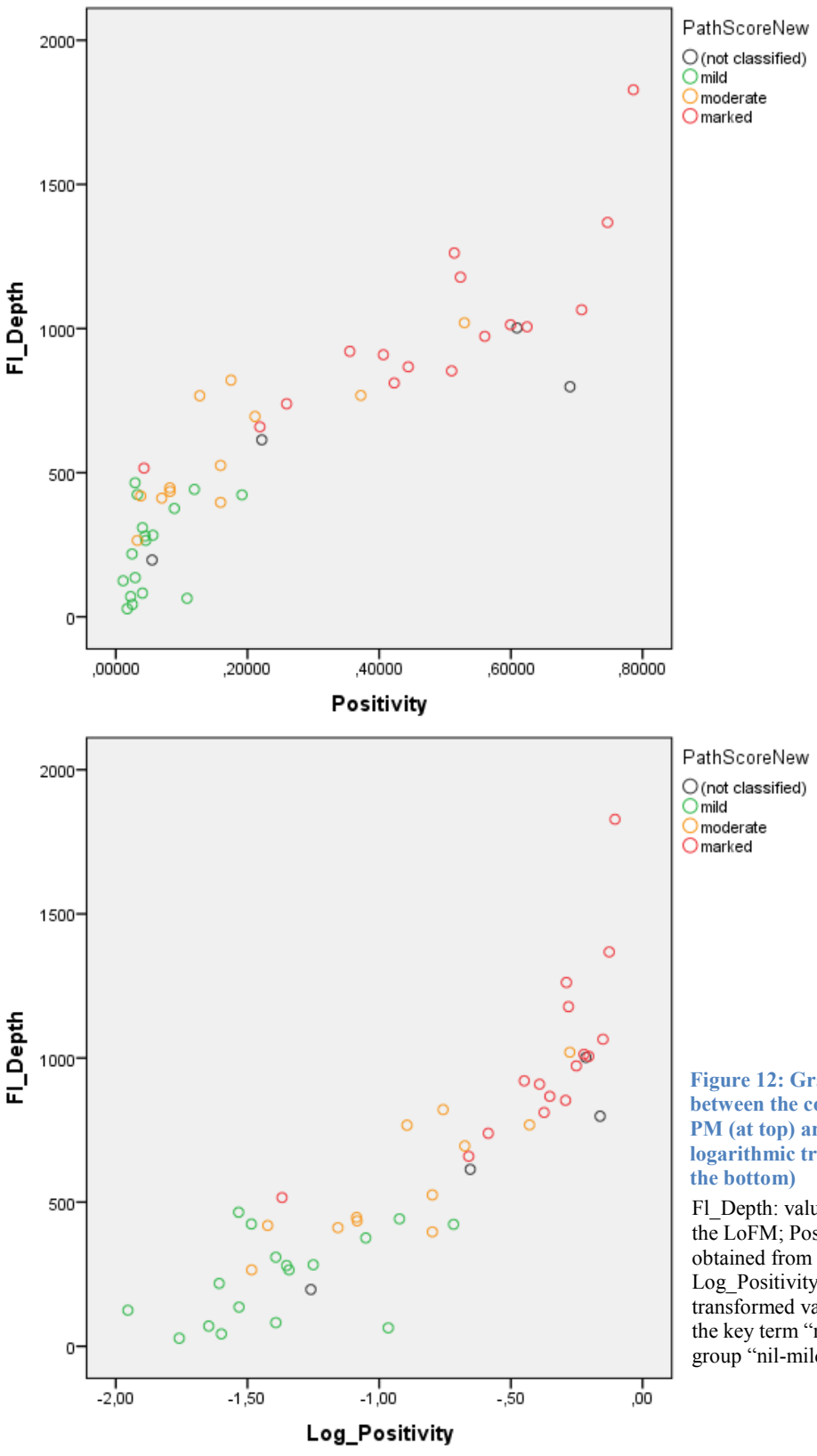

Figure 12: Graphical comparison between the correlations LoFM & PM (at top) and LoFM & logarithmic transformed PM (at the bottom)

Fl_Depth: values obtained from the LoFM; Positivity: values obtained from the PM; Log_Positivity: logarithmic transformed values of Positivity; the key term "mild" refers to group "nil-mild"

4 Discussion

4.1 Methodological considerations

Several specimens were excluded from my analysis and different evaluation algorithms were created in order to balance inequalities in histological circumstances (see *Sections 2.4.2* and *2.5.1.2*). In the following section I further discuss the possibility of different histological processing effects and other sources of error.

LoFM

Vast differences in brightness of non-elastic fibres can be observed between different fluorescence microscopic images. As described in *Section 2.5.2* I identified the most superficial autofluorescent elastic fibres by comparing their brightness to the brightness of the tissue surrounding them. Consequently, the elastic fibres in those slides presenting with stronger fluorescence of non-elastic fibre tissue had to fluoresce stronger to exceed the brightness surrounding them compared to elastic fibres in slide with weak surrounding fluorescence levels. Hence, measurements of the depth of the most superficial autofluorescent elastic fibres might have been distorted by the fluorescence levels of tissue surrounding them.

Furthermore, in some fluorescence microscopic images the occurrence of clusters of thin, brightly fluorescing fibres was stated (*Section 2.5.2*). Not knowing their true origin and meaning I decided to exclude them since they did not create a continuous line parallel to the skin surface and hence did not indicate to represent the boundary between sun-damaged and healthy elastic fibre tissue.

By subjectively determining the level at which the autofluorescence of elastic fibres exceeds the fluorescence of tissue in their immediate surrounding this method's results are still dependent from the evaluator's subjective perception. After all, to some extent the LoFM might still not be entirely objective.

PM

The thicker the tissue sections are cut in slides stained with OES the longer the fractions of elastic fibres become and the higher the calculated positivity might become. At the same time, elastic fibres and fibres of other kind are more likely to lie on top of each other in

direction of the microscope's projection. Hence, the amount of elastic fibres obscured by other fibres and dermal tissue components might be elevated as well. When testing the algorithm OES2, the latter of these two effects seemed to have a greater impact on the analysis results leading to a decreased calculated positivity in thicker tissue sections. Trying to counterbalance this effect on the positivity I decided to apply a different, more sensitive analysis algorithm (OES3) to slides presenting with stronger Light Green counterstains. (For further considerations regarding different background intensities see *Section 2.5.1.2*)

One could argue that the application of two different analysis algorithms to quantify elastic fibres within OES slides contradicts the scientific principle of equal specimen treatment. Nonetheless, the establishment of two different algorithms was the necessary step to secure the comparability of all slides included in this method.

4.2 Statistical results

PM

Section 3.2 describes a high concordance between the positivity values obtained from the PM and the pathologists' evaluation, mathematically indicating a high reliability of this method. However, I would like to discuss one specific specimen's result: In *Section 3.1*, one sample assigned to class "marked" attracted attention by depicting an extraordinarily low positivity value. This sample, which I would like to refer to as "Sample X", was the only one of class "marked" to show a positivity within the range of values found in specimens classified as "nil-mild". Below (*Figure 13*) you can see the histological comparison between the H&E stained slides of this specimen and the specimen featuring the second lowest positivity result of class "marked", which for reasons of simplification I will refer to as "Sample Y".

Figure 13 depicts Sample Y with obvious solar elastosis (red arrow; faintly basophilic coarse fibres; see *Section 1.2.2.2*) whereas Sample X does not show any elastotic fibre but presents with fine collagen bundles and a rather wavy course of the dermo-epidermal junction. Comparing Sample X to the slide assigned to category "nil", more similarities can be observed. The observations regarding Sample X would rather fulfil the criteria of categories "nil" or "mild" than those of category "marked". (21)

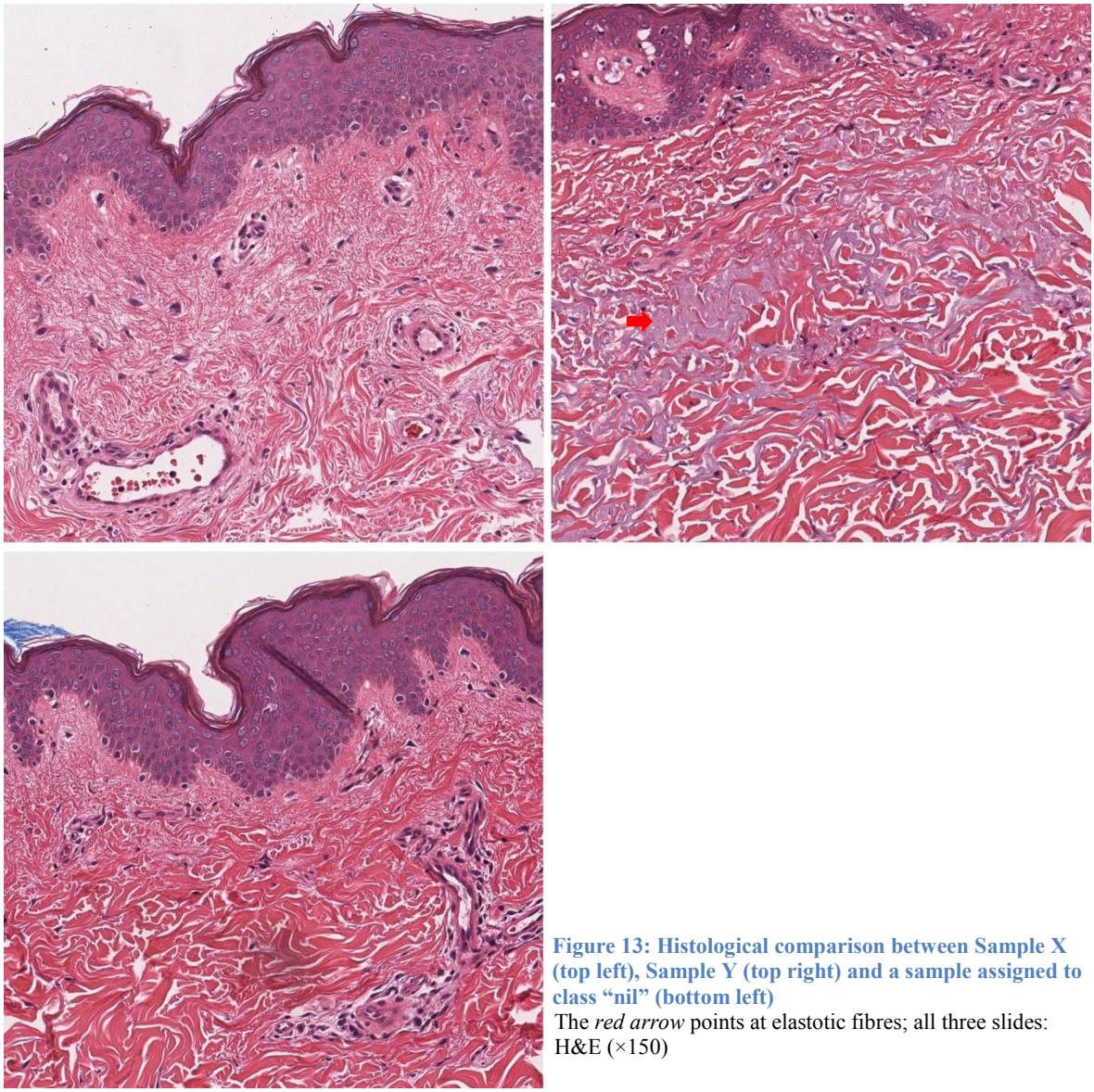

Figure 13: Histological comparison between Sample X (top left), Sample Y (top right) and a sample assigned to class "nil" (bottom left)
The *red arrow* points at elastotic fibres; all three slides: H&E (×150)

Questioning Sample X's correct assignment to class "marked", I conducted another ROC analysis excluding this single specimen. The obtained value limits stayed the same but presented with increased Youden's indexes (J) of 0.756 as limit between "nil-mild" and "moderate" and 0.931 as limit between "moderate" and "marked" (first ROC-analysis presented with J=0.727 and J=0.869, respectively).

In my opinion, the above considerations point out two things: Firsty, there is a strong association between the values obtained from the Positivity-Method and the pathologists' semiquantitative evaluations and secondly, if the PM's analysis algorithm is followed strictly, this method eliminates human failure as possible source of error.

LoFM

The best value limits between categories “nil-mild” and “moderate” and between categories “moderate” and “marked” were both calculated at the same depth, 490µm (see *Section 3.2*). Their accuracies were determined at a sensitivity of 78.6% and a specificity of 100% as limit between classes “nil-mild” and “moderate”, whereas the sensitivity and specificity of the value limit between classes “moderate” and “marked” was calculated at 100% and 79.3%, respectively.

These findings can be interpreted as follows: the depth of 490.5µm represents an ideal value limit between the classes “nil-mild” and “marked” since specificity and sensitivity are both 100% (J=1). Specimens assigned to class “moderate” spread rather evenly around this value limit. *Figure 10* on *page 47* in *Section 3.1* actually shows that six specimens assigned to this class have higher values and another six have lower values than 490.5µm. Hence, the distribution of “moderate” specimens centres at the value limit of 490.5µm.

As described in *Section 1.4* this thesis does not aim at establishing value limits between the categories established by pathologists. By calculating value limits and testing them for their accuracy I was trying to determine if the two quantitative methods established in this thesis correlate with the evaluations of pathologists. Considering the statistical results from this point of view, the Loss of Fluorescence-Method reflects well the pathologists’ assessments.

Correlation between the quantitative methods

The Pearson product-moment correlation coefficient being very high (0.899; see *Section 3.3*) indicates a linear correlation between the two quantitative methods established. Some authors even define correlation coefficients between 0.8 and 1.0 as strong to perfect. (49) Obviously, the logarithmic transformation of the values obtained from the PM did not further improve the degree of linear correlation.

4.3 Conclusions

In this diploma thesis I have established two histological methods to objectively quantify the degree of accumulated UVR damage in samples of human skin. I have demonstrated that both the PM and the LoFM delivered values which were largely in line with the evaluations conducted by experienced dermatopathologists. Furthermore, by establishing

precise algorithms, I have minimised the possible impact of human error and streamlined productivity within the pathological processing of skin samples.

Extrinsic skin aging, as described in *Section 1.2.2*, does not only emerge due to solar irradiation but is also caused by smoking and to a lesser degree air pollution. (12,13,17) Since the methods established quantify histological alterations, they do not help differentiate between causal relationships but determine the accumulated impact of overall exposure to miscellaneous risk factors.

Taken together, the two methods described in this thesis represent objective and quantitative alternatives to the currently established approach of pathologists who subjectively gauge the degree of CSD in skin samples and usually assign them to predefined semiquantitative categories.

Bibliography

(1) Rassner G. Dermatologie - Lehrbuch und Atlas. 9th ed. München: Urban & Fischer in Elsevier; 2009.

(2) Lüllmann-Rauch R. Taschenlehrbuch Histologie. 3rd ed. Stuttgart: Thieme; 2009.

(3) Welsch U. Haut. In: Welsch U, editor. Lehrbuch Histologie. 4th ed. München: Urban & Fischer in Elsevier; 2014. p. 539-558.

(4) Bruckner-Tuderman L. Biology of the Extracellular Matrix. In: Bolognia JL, Jorizzo JL, Schaffer JV, editors. Dermatology. 3rd ed. Edinburgh: Saunders; 2012. p. 1585-1640.

(5) Hwang KA, Yi BR, Choi KC. Molecular mechanisms and in vivo mouse models of skin aging associated with dermal matrix alterations. Lab Anim Res 2011 Mar;27(1):1-8.

(6) Cotta-Pereira G, Guerra Rodrigo F, Bittencourt-Sampaio S. Oxytalan, elaunin, and elastic fibers in the human skin. J Invest Dermatol 1976 Mar;66(3):143-148.

(7) Heo YS, Song HJ. Characterizing cutaneous elastic fibers by eosin fluorescence detected by fluorescence microscopy. Ann Dermatol 2011 Feb;23(1):44-52.

(8) Moc I, Horn F. Extrazellulärsubstanz - was zwischen den Zellen ist. In: Horn F, editor. Biochemie des Menschen - das Lehrbuch für das Medizinstudium Stuttgart ; New York, NY: Thieme; 2009. p. 455-460.

(9) Wang W, Lazar A. Diseases of collagen and elastic tissue. In: Calonje E, Brenn T, Lazar A, McKee PH, editors. McKee's pathology of the skin; with clinical correlations. 4th ed. Philadelphia: Elsevier Saunders; 2012. p. 935-966.

(10) Hausstein U, Mittag M. Bindegewebskrankheiten. In: Kerl H, Garbe C, Cerroni L, Wolff HH, editors. Histopathologie der Haut Berlin, Heidelberg: Springer; 2003. p. 455-475.

(11) Lever WF, Schaumburg-Lever G. Histopathology of the skin. 6th ed. Philadelphia: Lippincott; 1983.

(12) James WD, Berger TG, Elston DM. Andrews' Diseases of the Skin; Clinical Dermatology. 11th ed. Philadelphia ; London: Saunders Elsevier; 2011.

(13) DeLeo VA, Maso MJ. Photosensitivity. In: Moschella SL, Hurley HJ, editors. Dermatology. 3rd ed. Philadelphia; London; Toronto; Montreal; Sydney; Tokyo: Saunders; 1992. p. 507-532.

(14) Patterson JW. Weedon's skin pathology. 4th ed. London: Churchill-Livingstone Elsevier; 2016.

(15) Fenske NA, Lober CW. Aging and its Effects on the Skin. In: Moschella SL, Hurley HJ, editors. Dermatology. 3rd ed. Philadelphia; London; Toronto; Montreal; Sydney; Tokyo: Saunders; 1992. p. 107-122.

(16) Shames BS, Fretzin D. Disorders of Collagen, Elastin, and Ground Substance. In: Moschella SL, Hurley HJ, editors. Dermatology. 3rd ed. Philadelphia; London; Toronto; Montreal; Sydney; Tokyo: Saunders; 1992. p. 1269-1311.

(17) Vierkötter A, Krutmann J. Environmental influences on skin aging and ethnic-specific manifestations. Dermatoendocrinol 2012 Jul 1;4(3):227-231.

(18) Lim HW, Hawk JLM. Photodermatologic Disorders. In: Bolognia JL, Jorizzo JL, Schaffer JV, editors. Dermatology. 3rd ed. Edinburgh: Saunders; 2012. p. 1467-1486.

(19) Hadshiew I. Pigmentstörungen der Haut. In: Moll I, editor. Dermatologie. 7th ed. Stuttgart: Thieme; 2010. p. 478-488.

(20) Hasegawa K, Yoneda M, Kuwabara H, Miyaishi O, Itano N, Ohno A, et al. Versican, a major hyaluronan-binding component in the dermis, loses its hyaluronan-binding ability in solar elastosis. J Invest Dermatol 2007 Jul;127(7):1657-1663.

(21) Kvaskoff M, Pandeya N, Green AC, Perry S, Baxter C, Davis MB, et al. Solar elastosis and cutaneous melanoma: A site-specific analysis. Int J Cancer 2014 Nov 18.

(22) Meyers Lexikonredaktion, Bethge K editors. Schülerduden Physik. 3rd ed. Mannheim; Leipzig; Wien; Zürich: Dudenverlag; 1995.

(23) Rijken F, Bruijnzeel PLB. The pathogenesis of photoaging: the role of neutrophils and neutrophil-derived enzymes. J Investig Dermatol Symp Proc 2009 Aug;14(1):67-72.

(24) Bossi O, Gartsbein M, Leitges M, Kuroki T, Grossman S, Tennenbaum T. UV irradiation increases ROS production via PKCδ signaling in primary murine fibroblasts. J Cell Biochem 2008 Sep 1;105(1):194-207.

(25) Sander CS, Chang H, Salzmann S, Muller CS, Ekanayake-Mudiyanselage S, Elsner P, et al. Photoaging is associated with protein oxidation in human skin in vivo. J Invest Dermatol 2002 Apr;118(4):618-625.

(26) Yoshinaga E, Kawada A, Ono K, Fujimoto E, Wachi H, Harumiya S, et al. N^{ε}-(carboxymethyl)lysine modification of elastin alters its biological properties: implications for the accumulation of abnormal elastic fibers in actinic elastosis. J Invest Dermatol 2012 Feb;132(2):315-323.

(27) Bernstein EF. Reactive oxygen species activate the human elastin promoter in a transgenic model of cutaneous photoaging. Dermatol Surg 2002 Feb;28(2):132-135.

(28) Walker G, Hacker E. Ultraviolet Light as a Modulator of Melanoma Development. In: Murph M, editor. Research on Melanoma - A Glimpse into Current Directions and Future Trends: InTech; 2011. p. 198-228.

(29) Whiteman D, Green A. Epidemiology of Malignant Melanoma. In: Dummer R, Pittelkow MR, Iwatsuki K, Green A, Elwan NM, editors. Skin Cancer - A World-Wide Perspective. 1st ed. Heidelberg, Dortrecht, London, New York: Springer Berlin Heidelberg; 2011. p. 13-26.

(30) Gärtner R, Reincke M. Schilddrüse. In: Siegenthaler W, Blum HE, editors. Klinische Pathophysiologie. 9th ed. Stuttgart, New York: Georg Thieme Verlag; 2006. p. 270-290.

(31) Kamarashev JA, Schärer L, Zipser MC, Lockwood LL, Dummer R. Disease Entities: Malignant Melanoma. In: Dummer R, Pittelkow MR, Iwatsuki K, Green A, Elwan NM, editors. Skin Cancer - A World-Wide Perspective. 1st ed. Heidelberg, Dortrecht, London, New York: Springer Berlin Heidelberg; 2011. p. 169-185.

(32) Guggenheim M, Giovanoli P, Baumert BG, Eigentler TK, Garbe C, Mangana J, et al. Therapy - Melanoma. In: Dummer R, Pittelkow MR, Iwatsuki K, Green A, Elwan NM, editors. Skin Cancer - A World-Wide Perspective. 1st ed. Heidelberg, Dortrecht, London, New York: Springer Berlin Heidelberg; 2011. p. 307-342.

(33) Wick MR, Mills NC, Brix WK. Tissue procurement, processing, and staining techniques. In: Wick MR, editor. Diagnostic histochemistry. 1st ed. Cambridge: Cambridge University Press; 2008. p. 1-27.

(34) Lodish HF, Berk A, Kaiser CA, Krieger M, Bretscher A, Ploegh H, et al. Molecular cell biology. 7th ed. New York, NY: Freeman and Company; 2013.

(35) Alberts B, Johnson A, Lewis J, Raff M, Roberts K, Walter P. Molecular biology of the cell. 5th ed. New York, NY: Garland Science; 2008.

(36) Leica Biosystems Nussloch GmbH. X-tra® Slides. 2015; Available at: http://www.leicabiosystems.com/specimen-preparation/consumables/slides/adhesivepositively-charged-slides/details/product/x-traR-slides-1/. Accessed 1/21, 2015.

(37) Leica Biosystems Nussloch GmbH. Integrated Workstation Leica ST5010-CV5030 Workstation. 2015; Available at: http://www.leicabiosystems.com/routine-special-staining/routine-staining-coverslipping/details/product/leica-ts5015/. Accessed 1/18, 2015.

(38) Luna LG. Manual of histologic staining methods of the Armed Forces Institute of Pathology. 3rd ed. New York, NY: McGraw-Hill Book Company; 1968.

(39) Bancroft JD, Cook HC. Manual of Histological Techniques. Edinburgh ; New York: Churchill Livingstone; 1984.

(40) Burkhardt F. Besondere Arbeitsverfahren - Färbeverfahren. In: Burkhardt F, Bauernfeind A, editors. Mikrobiologische Diagnostik Stuttgart, New York: Thieme; 1992. p. 680-693.

(41) Mulisch M, Welsch U. Romeis - Mikroskopische Technik. 18th ed. Heidelberg: Spektrum Akad. Verl; 2010.

(42) Aperio ePathology. ScanScope® XT/XT2 System (data sheet). 2009.

(43) Leica Biosystems Nussloch GmbH. Aperio FL – Multiplexing, Immunofluorescence Slide Scanner. 2015; Available at: http://www.leicabiosystems.com/pathology-imaging/aperio-epathology/capture/details/product/leica-scanscope-fl/. Accessed 1/20, 2015.

(44) Leica Microsystems. Find your Filtercubes. 2015; Available at: http://www.leica-microsystems.com/products/light-microscopes/accessories/filtercubes-and-fluorochromes/find-your-filtercubes/. Accessed 1/19, 2015.

(45) Thermo Fisher Scientific Inc. Alexa Fluor® 488 dye. 2015; Available at: http://www.lifetechnologies.com/at/en/home/life-science/cell-analysis/fluorophores/alexa-fluor-488.html. Accessed 1/19, 2015.

(46) Aperio Technologies Inc. Positive Pixel Count Algorithm - User's Guide. 2009.

(47) GraphPad Software Inc. Statistics with Prism 6. 2015; Available at: http://www.graphpad.com/guides/prism/6/statistics/. Accessed 4/6, 2015.

(48) Weiß C. Basiswissen Medizinische Statistik. 6th ed. Berlin, Heidelberg: Springer; 2013.

(49) medistat GmbH. Medizinische Statistik | Datenanalyse & Statistische Beratung für Fachbereiche der Medizin. 2015; Available at: http://www.medistat.de/statistikberatung-glossar.php. Accessed 4/6, 2015.